JCI The Journal of Clinical Investigation

Inflammatory arthritis increases mouse osteoclast precursors with myeloid suppressor function

Julia F. Charles, … , Antonios O. Aliprantis, Mary C. Nakamura

J Clin Invest. 2012;122(12):4592-4605. https://doi.org/10.1172/JCI60920.

Research Article **Autoimmunity**

Increased osteoclastic bone resorption leads to periarticular erosions and systemic osteoporosis in RA patients. Although a great deal is known about how osteoclasts differentiate from precursors and resorb bone, the identity of an osteoclast precursor (OCP) population in vivo and its regulatory role in RA remains elusive. Here, we report the identification of a $CD11b^{-/lo}Ly6C^{hi}$ BM population with OCP activity in vitro and in vivo. These cells, which can be distinguished from previously characterized precursors in the myeloid lineage, display features of both M1 and M2 monocytes and expand in inflammatory arthritis models. Surprisingly, in one mouse model of RA (adoptive transfer of SKG arthritis), cotransfer of OCP with SKG $CD4^+$ T cells diminished inflammatory arthritis. Similar to monocytic myeloid-derived suppressor cells (M-MDSCs), OCPs suppressed $CD4^+$ and $CD8^+$ T cell proliferation in vitro through the production of NO. This study identifies a BM myeloid precursor population with osteoclastic and T cell–suppressive activity that is expanded in inflammatory arthritis. Therapeutic strategies that prevent the development of OCPs into mature bone-resorbing cells could simultaneously prevent bone resorption and generate an antiinflammatory milieu in the RA joint.

Inflammatory arthritis increases mouse osteoclast precursors with myeloid suppressor function

Julia F. Charles,[1,2,3] Lih-Yun Hsu,[1] Erene C. Niemi,[1,2] Arthur Weiss,[1,4] Antonios O. Aliprantis,[3] and Mary C. Nakamura[1,2]

[1]Department of Medicine, Division of Rheumatology, UCSF, San Francisco, California, USA. [2]Arthritis/Immunology Section, Veterans Administration Medical Center (VAMC), San Francisco, California, USA. [3]Department of Medicine, Division of Rheumatology, Allergy and Immunology, Brigham and Women's Hospital, Boston, Massachusetts, USA. [4]Howard Hughes Medical Institute, San Francisco, California, USA.

Increased osteoclastic bone resorption leads to periarticular erosions and systemic osteoporosis in RA patients. Although a great deal is known about how osteoclasts differentiate from precursors and resorb bone, the identity of an osteoclast precursor (OCP) population in vivo and its regulatory role in RA remains elusive. Here, we report the identification of a CD11b$^{-/lo}$Ly6C^{hi} BM population with OCP activity in vitro and in vivo. These cells, which can be distinguished from previously characterized precursors in the myeloid lineage, display features of both M1 and M2 monocytes and expand in inflammatory arthritis models. Surprisingly, in one mouse model of RA (adoptive transfer of SKG arthritis), cotransfer of OCP with SKG CD4$^+$ T cells diminished inflammatory arthritis. Similar to monocytic myeloid-derived suppressor cells (M-MDSCs), OCPs suppressed CD4$^+$ and CD8$^+$ T cell proliferation in vitro through the production of NO. This study identifies a BM myeloid precursor population with osteoclastic and T cell–suppressive activity that is expanded in inflammatory arthritis. Therapeutic strategies that prevent the development of OCPs into mature bone-resorbing cells could simultaneously prevent bone resorption and generate an antiinflammatory milieu in the RA joint.

Introduction

Osteoclasts are the primary bone-resorbing cell and are essential for physiologic bone remodeling. In the absence of either RANK or its ligand RANKL, the essential receptor-ligand pair for osteoclast differentiation and survival, mice lack osteoclasts and have severe osteopetrosis with absence of tooth eruption (1–3). Osteoclasts are myeloid lineage cells that also require M-CSF for differentiation and survival (4, 5). Osteoclasts can be cultured in vitro from BM, peripheral blood, or spleen cells in the presence of M-CSF and RANKL. Although BM CD11b$^{-/lo}$CD115$^+$CD117$^+$ cells are enriched in osteoclast differentiation activity (6, 7), the cell-surface phenotype and biology of the BM osteoclast precursor (OCP) and its relationship to other myeloid lineages has not been characterized in depth.

The common monocyte DC precursor (MDP) was described as having the cell-surface phenotype CD11b$^-$CD115$^+$CD117^{int} (8), and differentiation of monocytes and DCs from MDPs has been intensely studied (reviewed in ref. 9). It is likely that MDPs can also differentiate into osteoclasts, as a population with a similar surface phenotype is capable of differentiation into osteoclasts, macrophages, or DCs, depending on cytokine conditions (6, 10). Recent work confirmed the primary BM OCPs as CD11b$^{-/lo}$CD115$^+$CD117$^+$, although CD117$^-$ cells were also able to differentiate into osteoclasts less efficiently (6, 7). BM OCPs in the human *TNFA* Tg (hTNF-α–Tg) mouse were identified by others as characterized by the markers CD11b$^+$ and Gr-1$^-$, using the 1A-8 antibody that is specific for the granulocyte Ly6G receptor, the main component of the Gr-1 epitope (11). Recent studies have identified a circulating quiescent lineage committed OCP (QOP) also present in very low numbers in BM and identified by high expression of RANK (12). Other studies have suggested that immature DCs have the capacity to differentiate into functional osteoclasts in the presence of M-CSF and RANKL (13). Thus, we sought to further delineate the relationship of OCPs to defined myeloid precursors and monocyte subsets and to examine changes in the OCP population in inflammatory arthritis.

In the present study, we identify a BM CD11b$^{-/lo}$Ly6C^{hi} population that differentiates into osteoclasts in vitro as well as in vivo when adoptively transferred into ostecolast-deficient mice. These BM OCPs are distinct from MDPs, common DC precursors (CDPs), and monocyte subsets based on multiple cell-surface markers, including high Ly6C and absent-to-low CD11b expression. We find that the OCP population in the BM expands in inflammatory arthritis in the SKG mouse model. The phenotype of the OCP population as Ly6C^{hi} is notably similar to the described phenotype of some monocytic myeloid-derived suppressor cell (M-MDSC) populations. MDSCs are expanded in some autoimmune states, but have not been previously examined in inflammatory arthritis. We found that BM OCPs have MDSC function in vivo, in that cotransfer of OCPs with SKG CD4$^+$ T cells into *Rag*$^{-/-}$ recipients diminishes inflammatory arthritis compared with recipients receiving transfer of CD4$^+$ T cells alone. Mechanistically, OCPs suppressed T cell proliferation in vitro, a characteristic of MDSCs. While MDSCs have been characterized in tumor models, trauma, and other autoimmune diseases, they have not been directly demonstrated in inflammatory arthritis. Our study uniquely shows that inflammatory arthritis leads to expansion of BM myeloid OCP precursor cells and that the same myeloid OCP precursor cell population has both osteoclastogenic and MDSC function in vivo.

Conflict of interest: The authors have declared that no conflict of interest exists.

Citation for this article: *J Clin Invest.* 2012;122(12):4592–4605. doi:10.1172/JCI60920.

Results

SKG arthritis results in osteopenia and erosive bone lesions. SKG mice are BALB/c mice with a spontaneously arising point mutation in ZAP-70, leading to abnormal T cell selection and function (14). Following an innate immune stimulus such as zymosan injection, SKG mice develop a rheumatoid factor–positive, symmetric inflammatory peripheral arthritis clinically similar to RA in humans (15). Transfer of $CD4^+$ T cells is sufficient to induce SKG arthritis in lymphopenic hosts, and arthritis is dependent on IL-17, IL-6, IL-1, and TNF-α, which are also important in RA pathogenesis (14, 16). As in RA, BALB/c SKG mice develop both generalized osteopenia and localized joint erosions after the development of inflammatory arthritis. Microcomputed tomographic (μCT) analysis 14 weeks after arthritis onset demonstrated localized joint erosions in the ankle and phalanges (Figure 1A) and osteopenia at the proximal tibia metaphysis, with a significant decrease in bone volume/total volume (BV/TV) in arthritic SKG mice compared with healthy littermate controls (Figure 1B). Corresponding decreases in trabecular thickness and number and increased trabecular spacing were also seen (Supplemental Figure 1, A–C; supplemental material available online with this article; doi:10.1172/JCI60920DS1). Osteopenia was generalized and not purely periarticular, as demonstrated by cortical thinning of femoral midshaft (Figure 1C). Consistent with this significant bone loss, bone from SKG mice with chronic arthritis is reported to be mechanically fragile compared with that of age-matched BALB/c mice (17). Osteopenia in arthritic SKG mice is associated with increased osteoclast activity, as demonstrated by increased serum C-terminal telopeptide of collagen type I (CTX) after arthritis induction (Supplemental Figure 1D). Consistent with our findings, others have examined the SKG model of inflammatory arthritis by histology and 3D stereological methods and demonstrated increased osteoclast number and surface area in mice with 6 and 12 weeks of arthritis (18). We cannot rule out a contribution from decreased osteoblast activity, however, as is seen at sites of erosion in the serum transfer model of arthritis (19).

BM osteoclast differentiation potential increases with inflammatory arthritis. Consistent with increased serum CTX in arthritic mice, osteoclast differentiation from equal numbers of BM monocytes (BMMs) from control and arthritic mice 8 weeks after disease induction demonstrated enhanced osteoclastogenesis in arthritic mice (Figure 1D). Osteoclast differentiation from peripheral blood mononuclear cells also increased significantly in arthritic mice (Supplemental Figure 2A). Increased BM osteoclast differentiation potential in arthritic mice could result from increased numbers of precursor cells, increased sensitivity to differentiation stimuli, or both. As previous work suggests that arthritis increases the OCP pool (11, 20), we sought to identify myeloid subsets increased in arthritis and tested their capacity for osteoclast differentiation.

$CD11b^{-/lo}Ly6C^{hi}$ myeloid cells increase in arthritis and are OCPs. Utilizing flow cytometry with antibodies to CD11b, Gr1, Ly6C, and Ly6G (markers that distinguish murine monocyte phenotypes), we examined BM of SKG mice at 8 weeks of arthritis compared with healthy SKG controls. In addition to increases in the percentage of $CD11b^+Ly6C^{hi}$ inflammatory monocytes, we observed a $CD11b^{-/lo}Ly6C^{hi}$ population consisting of approximately 1% of total BM that increases reproducibly with arthritis to approximately 3%. This population is further characterized as $Ly6G^-$ and $Gr1^+$ (Figure 1E). Culture of $CD11b^{-/lo}Ly6C^{hi}$ cells isolated by FACS from SKG BM depleted for $CD3/B220/Ter119^+$ cells demonstrates that this population contains OCPs. The sorted $CD11b^{-/lo}Ly6C^{hi}$ population, 97.5% pure by flow cytometry, is highly enriched for osteoclast formation when cultured in M-CSF and RANKL compared with $CD3/B220/Ter119^-$ BM (Figure 1F). Both the percentage and total number of $CD11b^{-/lo}Ly6C^{hi}$ cells increases significantly in BM from SKG arthritic mice 8 weeks after injection with zymosan, compared with age-matched BALB/c controls or healthy nonarthritic SKG littermates (Figure 1G). This increase in OCPs can be seen as early as 1 week after zymosan injection, prior to the development of synovial inflammation (Supplemental Figure 2B). Thus, the $CD11b^{-/lo}Ly6C^{hi}$ population is induced by arthritis and contains OCP potential.

$CD11b^{-/lo}Ly6C^{hi}$ cells are the primary OCP-containing population in BM independent of strain background. Plasticity is a common feature of myeloid lineage populations, and it is possible that other myeloid populations could function as OCPs in vitro. Thus, we compared the osteoclast differentiation potential of $CD11b^{-/lo}Ly6C^{hi}$ cells with that of other myeloid cell populations. Four myeloid populations were isolated from CD3/B220/Ter119-depleted BM from nonarthritic SKG mice by FACS sorting based on CD11b and Ly6C surface expression, as shown in the dot plot in Figure 2A. Cells were cultured in M-CSF and RANKL either on plastic for TRAP staining on day 3 (Figure 2B) or on a calcium phosphate monolayer to examine resorption on day 14 (Figure 2C). The $CD11b^{-/lo}Ly6C^{hi}$ population contained the majority of OCPs, consistent with the findings of Jacquin et al. that OCPs are $CD3^-B220^-CD11b^{-/lo}$ (7). The $CD11b^{-/lo}Ly6C^{hi}$ OCP population is heterogeneous for CD11b expression, and both $CD11b^-$ and $CD11b^{lo}$ cells form osteoclasts in vitro, although the $CD11b^-$ population is more efficient (Supplemental Figure 2). This is consistent with recent findings that CD11b can negatively regulate osteoclastogenesis (21). Osteoclasts generated from sorted $CD11b^{-/lo}Ly6C^{hi}$ OCPs are functional because they are $TRAP^+$ and capable of resorbing a calcium phosphate monolayer (Figure 2, B and C). $CD11b^{-/lo}Ly6C^{hi}$ cells also formed osteoclasts in coculture with primary osteoblasts (Figure 2, D and E). The quadruple-negative (QN) ($CD3^-B220^-CD11b^-Ly6C^-$) population also contained some limited capacity to differentiate into functional osteoclasts. MDPs, which have been described as differentiating into osteoclasts, fall within this gate. The $B220^+$ and $CD3^+$ populations did not contain any osteoclast differentiation capacity (J.F. Charles, unpublished observations).

As SKG mice have an osteopenic bone phenotype compared with wild-type and heterozygous littermate controls (Supplemental Figure 3) and others have reported that BM OCPs in C57BL/6 and hTNF-α–Tg are $CD11b^+Gr1^-$ (11), we sought to determine whether the $CD11b^{-/lo}Ly6C^{hi}$ OCP population was strain or SKG specific. We sorted BM myeloid populations from wild-type BALB/c and C57BL/6 mice and found that the surface phenotype of OCPs with the greatest differentiation capacity is $CD3^-B220^-CD11b^{-/lo}Ly6C^{hi}$ independent of background (Supplemental Figure 4).

The SKG model of inflammatory arthritis differs from the hTNF-α–Tg model in that it requires an innate immune stimulus to initiate arthritis and is characterized by high IL-6, IL-1, and Th17 cell activity in addition to elevated TNF-α. TNF-α is proosteoclastogenic both directly through activation of NF-κB and indirectly via upregulation of RANKL on mesenchymal cells (22) and could potentially alter the ability of myeloid precursors to differentiate into osteoclasts. We thus examined whether OCPs in TNF-α–driven disease differ from OCPs in SKG arthritis. Utilizing the same FACS sorting protocol to analyze BM of heterozygous

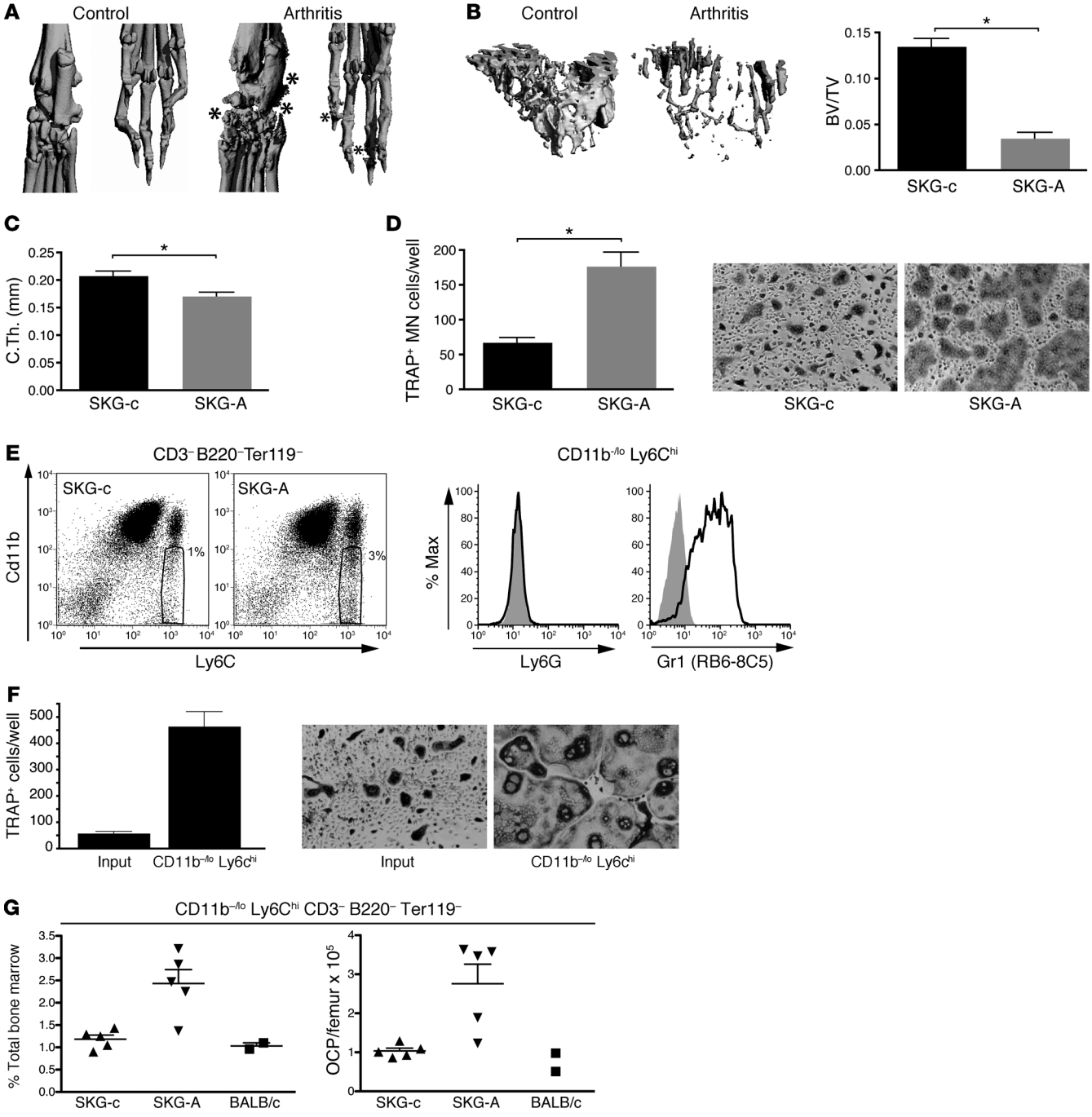

Figure 1

Erosive arthritis, generalized bone loss, and increased BM OCPs in SKG arthritis. (**A**–**C**) μCT analysis of female SKG mice with chronic arthritis (SKG-A) compared with healthy littermate controls (SKG-c) shows erosions and generalized bone loss. (**A**) Representative 3D reconstructions of rear paw, showing erosions (asterisks) and (**B**) representative images and quantitation of BV/TV of proximal tibia metaphysis and (**C**) cortical thickness, $n = 4$ per group. $^*P \leq 0.03$, Mann-Whitney test. (**D**) BM from SKG mice after 8 weeks arthritis shows increased osteoclast differentiation. BM cells derived from arthritic or control SKG mice, $n = 4$ each group, were cultured in M-CSF and RANKL and number of TRAP-stained multinuclear (MN) osteoclasts were quantified from triplicate wells of 2.5×10^3 cells plated from each individual, $P = 0.03$ Mann-Whitney test. A representative image of TRAP-stained cultures is shown. Original magnification, ×10. Data are representative of 3 experiments. (**E**) Representative dot plot showing an increased BM B220$^-$CD3$^-$CD11b$^{-/lo}$Ly6C^{hi} population in arthritic mice. Surface phenotype of CD11b$^{-/lo}$Ly6C^{hi} cells is Ly6G$^-$ Gr1$^+$. (**F**) CD11b$^{-/lo}$Ly6C^{hi} cells sorted from SKG BM are enriched for OCPs compared with the CD3$^-$B220$^-$Ter119$^-$ input; triplicate cultures of 12.5×10^3 cells were plated in M-CSF and RANKL for 3 days. Representative images are shown. Original magnification, ×10. (**G**) The CD11b$^{-/lo}$Ly6C^{hi} population increases in percentage (top) and total number (bottom) in SKG mice after 8 weeks arthritis compared with healthy littermate controls or age-matched BALB/c controls. $P < 0.005$, 1-way ANOVA. Representative data from 3 independent experiments are shown.

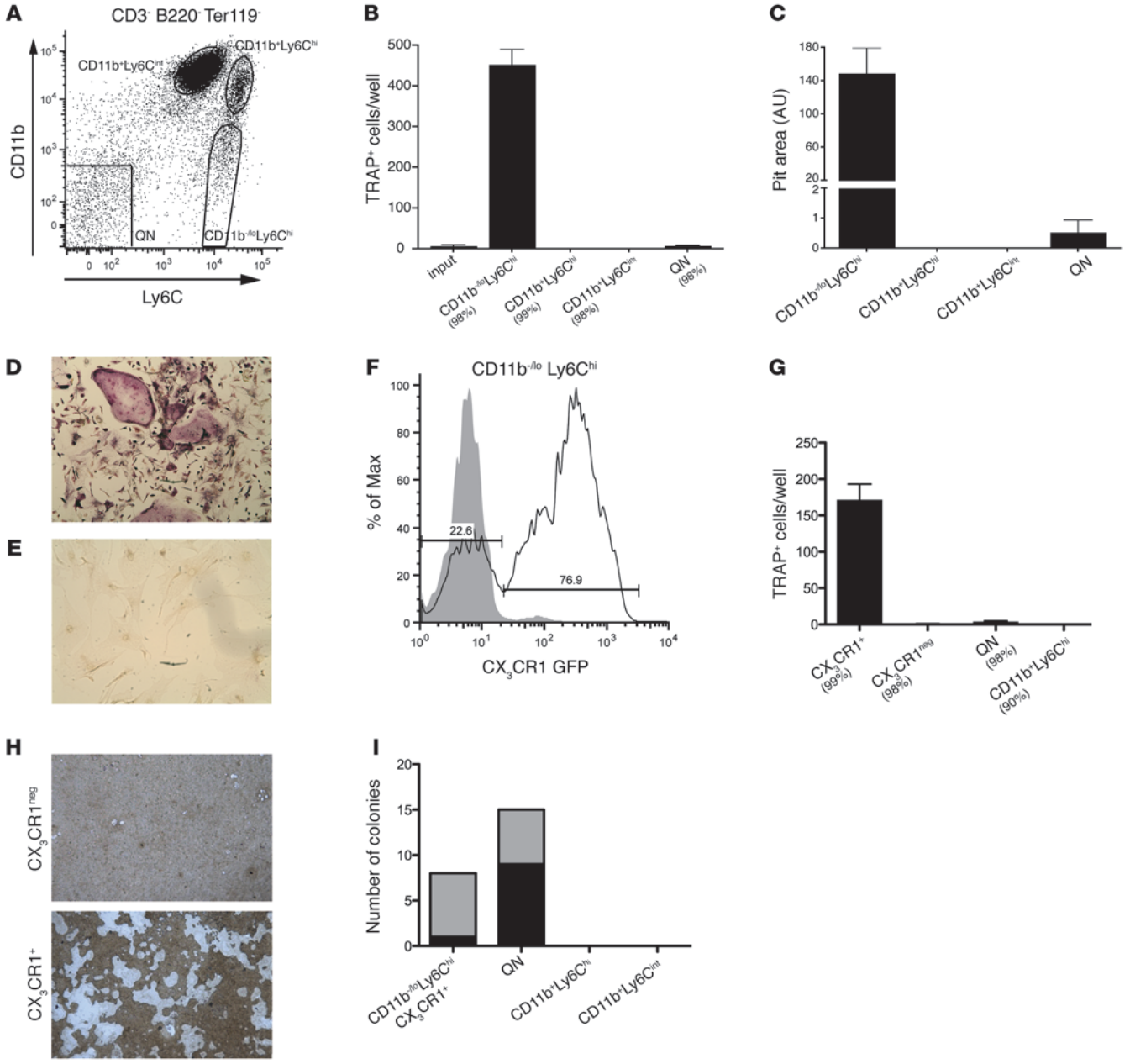

Figure 2

The CD11b$^{-/lo}$Ly6C^{hi}CX$_3$CR1$^+$ population contains the majority of osteoclast precursor activity. (**A**–**C**) Individual BM populations from SKG mice, sorted by CD11b and Ly6C staining as illustrated in **A**, were plated in triplicate at 2.5 × 10^3/well in M-CSF and RANKL. (**B**) Multinucleated TRAP$^+$ cells were counted after 3 days, and (**C**) resorption pits on osteologic slides were quantitated after 14 days culture. The purity of each sorted population is stated in parenthesis in the *x* axis label. Results are representative of 4 independent experiments. (**D**) TRAP staining of CD11b$^{-/lo}$Ly6C^{hi} OCPs cocultured with BM stromal cell–derived osteoblasts demonstrates osteoclast formation that is absent in parallel osteoblast-only culture. (**E**) Original magnification, ×10. (**F**) CX$_3$CR1 expression is variable in the CD11b$^{-/lo}$Ly6C^{hi} population. CX$_3$CR1 expression by CD11b$^{-/lo}$Ly6C^{hi}CD3$^-$B220$^-$Ter119$^-$ gated BM from CX$_3$CR1-GFP^{het} mice (black line) compared with C57BL/6 (gray area). (**G**) Triplicate cultures of 1 × 10^3 cells/well in M-CSF and RANKL demonstrates that only the CX$_3$CR1$^+$CD11b$^{-/lo}$Ly6C^{hi} population efficiently differentiates into multinucleated TRAP$^+$ osteoclasts and (**H**) forms resorption pits on osteologic slides. Original magnification, ×4. Results are representative of 3 replicates. (**I**) CD11b$^{-/lo}$Ly6C^{hi}CX$_3$CR1$^+$ cells retain the ability to form osteoclast after long-term culture. The total number of colonies obtained from single cells sorted from the indicated populations after 60 days in culture is indicated by column height, with the number retaining osteoclast differentiation capacity denoted in gray.

TNF-α–Tg mice with arthritis, we found that CD11b$^{-/lo}$Ly6C^{hi} are the primary OCP population in TNF-α–Tg mice and the number of OCPs in arthritic mice is increased compared with that in C57BL/6 controls (Supplemental Figure 4).

OCPs express CX$_3$CR1, the fractalkine receptor. The BM OCPs we identified are distinguished from MDPs and CDPs by expression of Ly6C, a marker of inflammatory monocytes (9), and from monocytes by virtue of low CD11b expression. CX$_3$CR1, the frac-

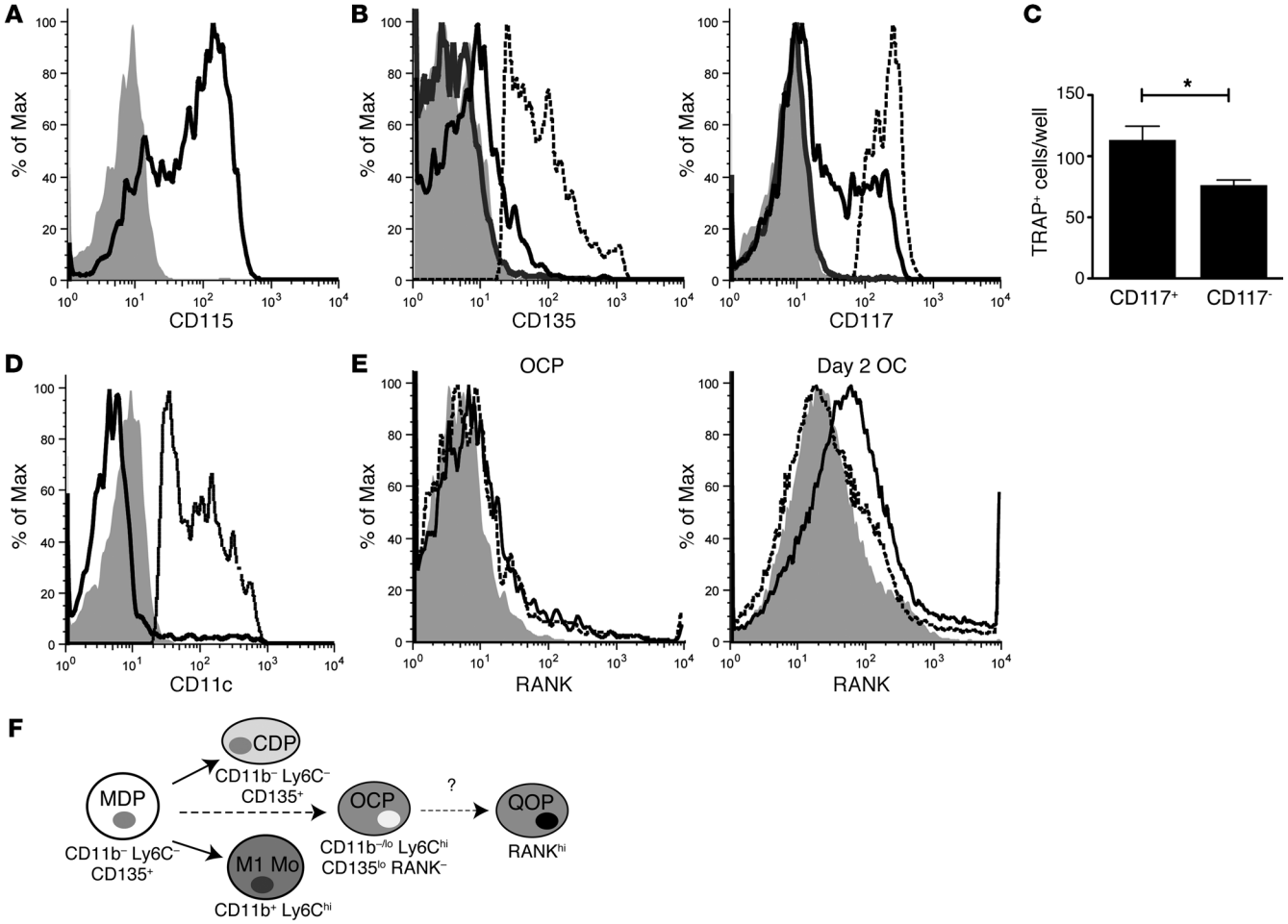

Figure 3

CD11b$^{-/lo}$Ly6C^{hi}CX$_3$CR1$^+$ OCPs are distinct from other myeloid precursors. (**A**–**C**) FACS analysis of cell-surface markers on CD3$^-$B220$^-$Ter119$^-$ gated BM from CX$_3$CR1-GFP^{het} distinguishes OCP from other myeloid populations. Staining of CD11b^{lo}Ly6C^{hi} CX$_3$CR1 OCP population with the indicated antibody (lines) compared with isotype control (gray area) is shown. (**A**) OCPs are predominantly CD115$^+$. (**B**) OCPs are CD135^{lo}CD117$^{+/-}$, further distinguishing them from CD11b$^-$Ly6C$^-$MDPs (CD135$^+$CD117$^+$, dashed line) and CD11b$^+$Ly6C^{hi} M1 monocytes (CD135$^-$ CD117$^-$, dark gray line). (**C**) Both CD117$^+$ and CD117$^-$ subsets are capable of differentiating into osteoclasts in vitro, although those in the CD117$^+$ subset are more efficient. TRAP$^+$ multinuclear osteoclast formed per 1 × 10^3 cells cultured in triplicate in M-CSF/RANKL, *P = 0.03. (**D**) OCPs are CD11c$^-$, in contrast with pre-DCs (CD11b$^+$CX$_3$CR1$^+$CD11c$^+$, dotted line). (**E**) GST-RANKL-biotin (black line) or GST-biotin control (gray area) demonstrate RANK expression on the surface of BM-derived day 2 osteoclasts (right panel) but not OCPs (left panel). Loss of osteoclast-binding RANKL-GST-bio binding in the presence of excess unlabeled RANKL (dashed line) demonstrates specificity. (**F**) Model of myeloid differentiation with the CD11b$^{-/lo}$Ly6C^{hi}CX$_3$CR1$^+$CD115$^+$ OCP as distinct myeloid precursors derived from MDPs; Mo, monocyte; QOP, lineage committed QOP.

talkine receptor, is expressed by many myeloid cell types, including MDPs, and is expressed by migrating OCPs in vivo (23). To further characterize the surface phenotype of the OCP population, we examined expression of CX$_3$CR1 within the population. CX$_3$CR1 expression varied within the CD11b$^{-/lo}$Ly6C^{hi} population, with up to approximately 20% of the cells being CX$_3$CR1$^-$ (Figure 2F). Culture of subpopulations within CD11b$^{-/lo}$Ly6C^{hi} OCPs, isolated based on CX$_3$CR1 status, demonstrated that only CX$_3$CR1$^+$CD11b$^{-/lo}$Ly6C^{hi} differentiate into functional osteoclasts (Figure 2, G and H).

We were further interested in exploring the clonogenic potential of the OCP population identified. CX$_3$CR1$^+$CD11b$^{-/lo}$Ly6C^{hi} cells were sorted at 1 cell per well into 96-well plates and expanded in medium containing 5% conditioned supernatant from CMG14-12 cells (CMG) as a source of M-CSF for 60 days. Cells were then replated in 5% CMG supplemented with 25 ng/ml RANKL and cultured for 5 days. A subset of colonies formed from CX$_3$CR1$^+$CD11b$^{-/lo}$Ly6C^{hi} cells retained the ability to differentiate into osteoclasts (Figure 2I). Thus, our data indicate that the OCP population we have identified is heterogenous, both by CD11b staining and the ability to differentiate into osteoclasts. Consistent with the QN population containing early myeloid precursors, some colonies from single QN cells also retained osteoclast differentiation ability. In contrast, no osteoclast-forming colonies could be derived from CD11b$^+$Ly6C^{int} or CD11b$^+$Ly6C^{hi} cells.

CX$_3$CR1$^+$CD11b$^{-/lo}$Ly6C^{hi} OCPs are distinct from other BM myeloid precursor populations. Like the earlier myeloid precursor MDPs, OCPs expressed the M-CSF receptor CD115/c-fms (Figure 3A). In contrast

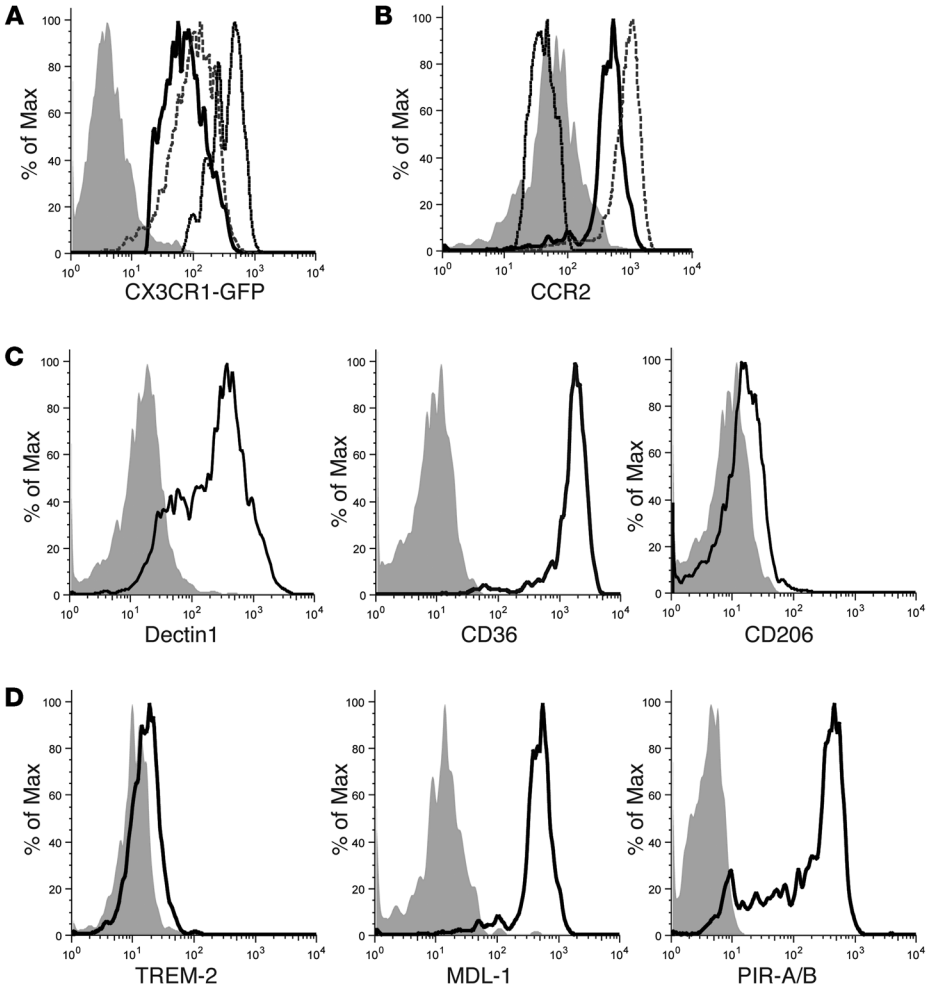

Figure 4
$CD11b^{-/lo}Ly6C^{hi}CX_3CR1^{+}$ OCPs have both M1 and M2 characteristics and express many osteoclast-associated receptors. (**A**) CX_3CR1 expression assessed by GFP intensity in C57BL/6 $CX_3CR1\text{-}GFP^{het}$ BM demonstrates that $CD11b^{-/lo}Ly6C^{hi}CX_3CR1^{+}$ OCP (black line) have CX_3CR1 expression levels similar to those of M1 monocytes ($CD11b^{+}Ly6C^{hi}CD117^{-}$, gray dashed line) and considerably lower than those of M2 monocytes ($CD11b^{+}Ly6C^{lo}CD117^{-}$, dotted line). (**B**) CCR2 surface expression on OCP (black line) is positive compared with $CD11b^{+}Ly6C^{lo}$ $CCR2^{-}$ M2 monocytes (dotted line), but lower than $CD11b^{+}Ly6C^{hi}$ M1 monocytes (gray dashed line). α-CCR2 antibody staining of OCP from *Ccr2*$^{-/-}$ mice (gray area) is shown as a staining control. (**C**) OCPs express markers of M2 lineage, including Dectin1, CD36, and CD206. (**D**) OCPs express innate immune receptors previously reported to affect osteoclast function. Staining with antibodies to TREM-2, MDL-1, and PIRA/B (black line) are shown compared with isotype control (gray area).

to MDPs, however, OCPs had low expression of CD135/Flt3 and contained both CD117/c-Kit–positive and –negative/low–expressing populations (Figure 3B). Further sorting the OCP population, based on CD117 expression, demonstrated that both $CD117^{+}$ and the $CD117^{-}$ OCPs differentiate into osteoclasts, although the $CD117^{+}$ population was more efficient (Figure 3C). As immature DCs can differentiate into osteoclasts in vitro and are incorporated into multinucleated giant cells at sites of bone erosion in vivo (13, 24), we looked at CD11c expression on OCPs and found that, unlike BM pre-DCs, OCPs are $CD11c^{-}$ (Figure 3D). We hypothesize that the $CX_3CR1^{+}CD11b^{-/lo}Ly6C^{hi}$ population with OCP capacity is a distinct myeloid precursor population, distinguished from other BM precursors by their pattern of CD11b and Ly6C expression. Analogous to CDPs, OCPs may derive from MDPs, which are also capable of forming osteoclasts in vitro, but can be distinguished from MDPs and CDPs by low CD135 expression (Figure 3F).

Like other myeloid cell types, OCPs demonstrate differentiation plasticity in vitro. Plasticity is a hallmark of the myeloid lineage. In some circumstances, monocytes can differentiate into inflammatory DCs or macrophages (9), and as discussed above, CDPs can give rise to osteoclasts in vitro. We tested whether $CD11b^{-/lo}Ly6C^{hi}CD117^{+}$ OCPs are similarly plastic by examining their phenotype following culture under conditions promoting macrophage and DC development. After 8 days of culture in M-CSF, sorted OCPs become uniformly CD11b and F4/80 high, suggesting a macrophage phenotype (Supplemental Figure 5A). OCP-derived macrophages are functional, as demonstrated by active phagocytosis of Alexa Fluor 488–labeled zymosan A particles (Supplemental Figure 5, B and C). Similarly, sorted OCPs cultured in GM-CSF became predominantly $CD11c^{+}$ and expressed MHCII (Supplemental Figure 5, D and E). Thus, $CD11b^{-/lo}Ly6C^{hi}CD117^{+}$ OCPs are likely earlier in the osteoclast differentiation pathway than the recently described lineage-committed QOPs, which fail to differentiate into DCs, but retain some ability to differentiate into macrophages (12). Although OCPs display multilineage plasticity in vitro, their in vivo capacity to differentiate into other myeloid lineages remains to be tested.

OCPs do not express RANK and are distinct from lineage-committed QOPs. Immediately upon isolation from the BM, RANK expression on OCPs, as detected by binding of GST-RANKL-biotin, is negligible (Figure 3E), and quantitative PCR (qPCR) for RANK expression using validated primers does not detect transcript above no RT control (J.F. Charles, unpublished observations). GST-RANKL-biotin binding can be readily detected, however, on day 2 osteoclasts, and this binding is specific, as it can be inhibited by preincubation with excess unlabeled RANKL (Figure 3E). This is distinct from QOPs, which are reported to be $RANK^{hi}$ in the BM (12). Further data contrasting our OCP population with

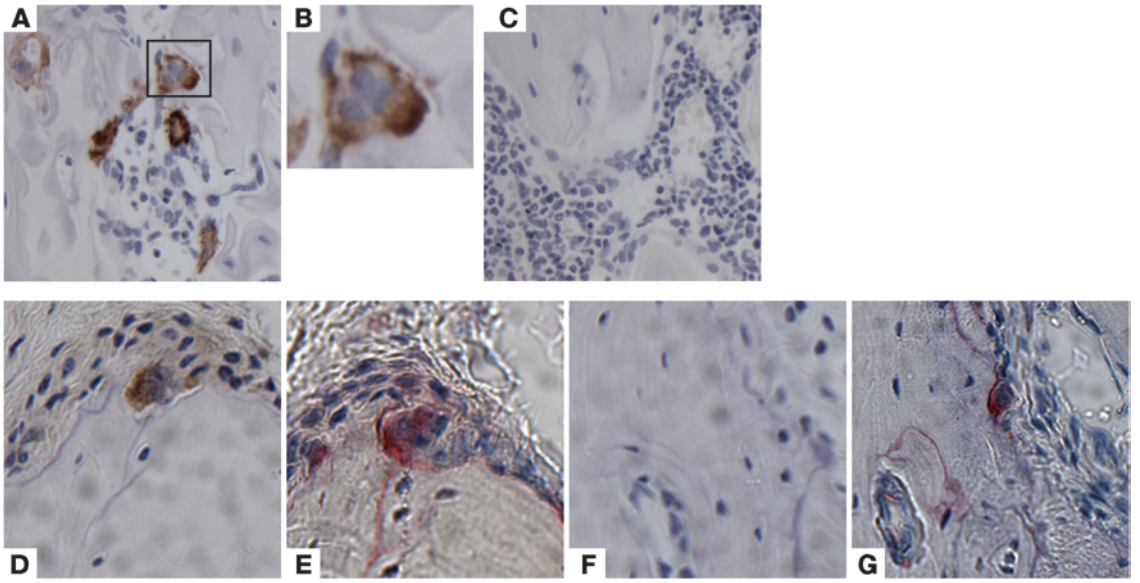

Figure 5
BM CD11b$^{-/lo}$Ly6C^{hi}CD117^{+} OCPs differentiate into osteoclasts in vivo. (**A**–**C**) Intramedullary injection of *mT/mG^{OC}* OCPs into *nfatc1$^{\Delta/\Delta}$* femurs demonstrates that CD11b$^{-/lo}$Ly6C^{hi}CD117^{+} are bona fide osteoclast precursors. (**A**) Donor-derived cathepsin K^{+} GFP^{+} osteoclasts are detected by anti-GFP immunohistochemistry (IHC) on femurs of *nfatc1$^{\Delta/\Delta}$* mice 7 days after intramedullary injection of OCP; (**B**) Enlargement of boxed area in **A**, demonstrating multinucleation of donor-derived cells. (**C**) No GFP^{+} osteoclasts were present in control mice injected with C57BL/6 OCPs. (**D**–**G**) Intravenous injection of *mT/mG^{OC}* OCP into C57BL/6 mice 24 hours after calvarial LPS injection. (**D**) Anti-GFP IHC on calvarial sections 4 days after cell transfer demonstrates donor-derived cathepsin K^{+} GFP^{+} osteoclasts that also stain for TRAP (**E**). No GFP signal is detected in no–cell transfer control animals (**F**), although TRAP^{+} multinucleated cells can be detected (**G**). Counterstain, hematoxylin. Original magnification, ×40 (**A**, **C**–**G**); ×300 (**B**).

QOP include observations that OCPs (a) contain Ki-67–positive cells upon isolation from the BM (Supplemental Figure 5F), (b) readily proliferate when exposed to M-CSF (Supplemental Figure 5G), and (c) display reduced osteoclast differentiation in the presence of hydroxyurea (Supplemental Figure 5H). Thus OCPs are a distinct precursor population, which we hypothesize reside at an earlier stage in the myeloid differentiation scheme than QOP (Figure 3F).

OCPs have features that are both M1 and M2 like. Data from in vitro studies has suggested that, analogous to the Th1/Th2 paradigm, macrophages polarize into M1 and M2 phenotypes, which can be characterized functionally and by cell-surface markers. M1, or classically activated, macrophages secrete proinflammatory cytokines, including TNF-α, and express high levels of iNOS. M2, or alternatively activated, macrophages are thought to have a reparative function, are implicated in wound healing, and express arginase and IL-10 (25, 26). CX_3CR1 expression on OCPs was similar to that of M1 monocytes (Figure 4A). We thus examined expression of CCR2, which can differentiate between M1- and M2-like phenotypes, on OCPs. Like M1 monocytes, OCPs are CCR2^{+}, though CCR2 expression was distinctly lower on OCPs (Figure 4B). Moreover, OCPs also expressed markers characteristic of the M2 phenotype, including Dectin1, CD36, and CD206 (Figure 4C). Thus, BM OCPs are neither clearly M1 nor M2 like, but have a mixed surface receptor phenotype.

OCPs express receptors with known roles in osteoclast differentiation. Many innate immune receptors modulate osteoclast differentiation and/or function through cosignaling with RANKL. We were interested to see whether these receptors are present on OCPs and found that receptors providing cosignaling through DAP12 and FcRγ were present on the OCP cell surface. Triggering receptor expressed on monocytes (TREM-2) and myeloid DAP12-associating lectin (MDL-1, also known as CLEC-5A), both DAP12-associated receptors, have been shown to costimulate osteoclast differentiation (27–29), and MDL-1 was recently implicated in osteoclast differentiation and inflammatory bone loss (30). TREM-2 levels on OCPs were quite low, while MDL-1 expression was high on OCPs (Figure 4D). OCPs also stained brightly with an antibody that recognizes both the paired immunoglobulin receptors A and B (PIR-A and PIR-B), implicated in FcRγ–mediated costimulation and inflammatory bone loss, and inhibitory signaling, respectively (Figure 4D and refs. 31, 32). OCPs are thus poised to receive costimulatory signals regulating osteoclast differentiation.

CD11b$^{-/lo}$Ly6C^{hi} OCPs differentiate into osteoclasts in vivo. In vitro differentiation assays can misrepresent physiologic lineage potential (33). Thus, to determine whether the CD11b$^{-/lo}$Ly6C^{hi} population is a bona fide OCP in vivo, we performed cell transfer experiments with the *mT/mG* reporter strain (34), in which a cassette containing floxed membrane–targeted tdTomato is inserted at the *RosA26* locus. In the presence of Cre recombinase, tdTomato is excised and a downstream membrane targeted EGFP is expressed. To track OCP differentiation in vivo, the *mT/mG* reporter was crossed to Tg mice where *Ctsk* is replaced with *Cre* (*Ctsk-Cre*) and the resulting mice (referred to hereafter as *mT/mG^{OC}*) were used as donors. *Nfatc1$^{\Delta\Delta}$* osteoclast-deficient hosts were generated by treating *Nfatc1$^{fl/fl}$ Mx1-Cre* mice with poly(I:C) (35). Intramedullary injection of *mT/mG^{OC}* OCPs into osteoclast-deficient *Nfatc1$^{\Delta\Delta}$* femurs resulted in the formation of multinucleated GFP^{+} (and thus

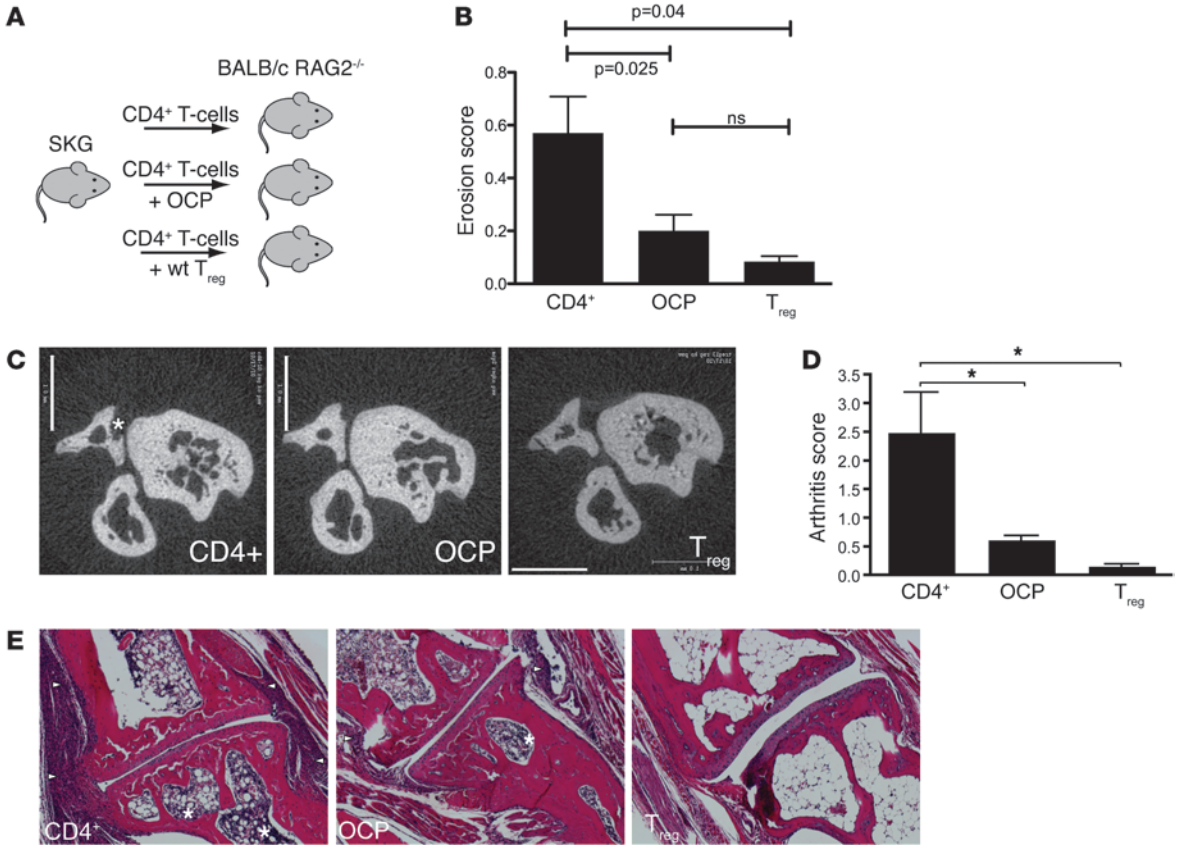

Figure 6

Adoptive transfer of CD11b$^{-/lo}$Ly6C^{hi} OCP does not increase erosive disease, but unexpectedly ameliorates inflammatory arthritis in the adoptive transfer SKG model. (**A**) Schematic of adoptive transfer experiment. Adoptive transfer of conventional SKG CD4$^+$CD25$^-$ T cells into *Rag2*$^{-/-}$ mice typically results in arthritis at 4 weeks. (**B**) One month after transfer, cross-sectional images from μCT of arthritic ankles were scored blindly for erosions. Coadoptive transfer of OCPs does not increase erosion score compared with mice receiving SKG CD4$^+$ cells alone. Few erosions are seen in the group receiving Tregs. (**C**) Representative cross-sectional images used for erosion scoring; star denotes an erosion. (**D**) Blinded arthritis scores are significantly ameliorated by coadoptive transfer of CD11b$^{-/lo}$Ly6C^{hi} OCP compared with CD4$^+$ group, although not as dramatically as with cotransfer of wild-type Tregs. *P = 0.03, Student's t test. (**E**) Representative images from sagittal ankle sections shows inflammatory changes in the marrow of both OCP and CD4$^+$ groups (stars), but more prominent synovial infiltrate (arrowheads) in the CD4$^+$ group. H&E staining. Original magnification, ×10.

cathepsin K expressing) cells adherent to bone surface detected by immunohistochemistry by 5 days after cell transfer (Figure 5, A and B). As a control, no GFP signal was seen when OCPs isolated from C57BL/6 mice (Figure 5C) or PBS (J.F. Charles, unpublished observations) were injected; furthermore, anti-GFP antibody does not detect tdTomato. Thus, OCPs give rise to osteoclasts in vivo. To confirm these findings, *mT/mG*^{OC} OCPs were administered intravenously 24 hours after inflammatory osteolysis was initiated by LPS injection into the calvaria of C57BL/6 mice. Donor-derived GFP$^+$, cathepsin K–expressing cells that were TRAP$^+$ and multinucleated, were detected 5 days after cell transfer (Figure 5, D and E). In contrast, no GFP signal was detected in control animals (Figure 5F) though host-derived TRAP$^+$ osteoclasts were identifiable in serial sections (Figure 5G). Thus, we have conclusively demonstrated that the CD11b$^{-/lo}$Ly6C^{hi}CD117$^+$ population is capable of giving rise to osteoclasts in physiologic and inflammatory models and is thus a bona fide OCP.

Adoptive transfer of OCPs reveals an unexpected immunomodulatory function. As a preliminary study of whether BM CD11b$^{-/lo}$Ly6C^{hi} OCPs promote osteoclast activity in vivo, we examined the effect of adoptive transfer of OCPs in an arthritis model. *Rag2*$^{-/-}$ mice develop inflammatory arthritis within 1 month after adoptive transfer of conventional CD4$^+$CD25$^-$ T cells from SKG mice, while coadoptive transfer of wild-type CD4$^+$CD25$^-$ and Tregs ameliorates disease (14, 36). We hypothesized that adoptive transfer of OCPs with conventional CD4$^+$ T cells would exacerbate erosive disease, while cotransfer of Tregs would diminish erosions along with decreasing disease severity. Splenic conventional CD4$^+$ T cells isolated from SKG mice were adoptively transferred into BALB/c *Rag2*$^{-/-}$ mice either alone or mixed with an equal number of wild-type Tregs or CD11b$^{-/lo}$Ly6C^{hi} OCPs isolated from SKG BM (Figure 6A). After 4 weeks, mice were assessed in blinded fashion for arthritis scores, and joints were analyzed for erosions by μCT and histology. As expected, coadoptive transfer of wild-type Tregs prevented the development of inflammatory, erosive arthritis (Figure 6, B and D) in mice receiving SKG CD4$^+$ T cells. However, coadoptive transfer of OCPs did not increase erosions, as detected by μCT (Figure 6, B and C), nor increase serum CTX, a measure of global resorptive activity (Supplemental Figure 6A). Unexpectedly, transfer of OCPs significantly ameliorated arthritis activity, though to a lesser

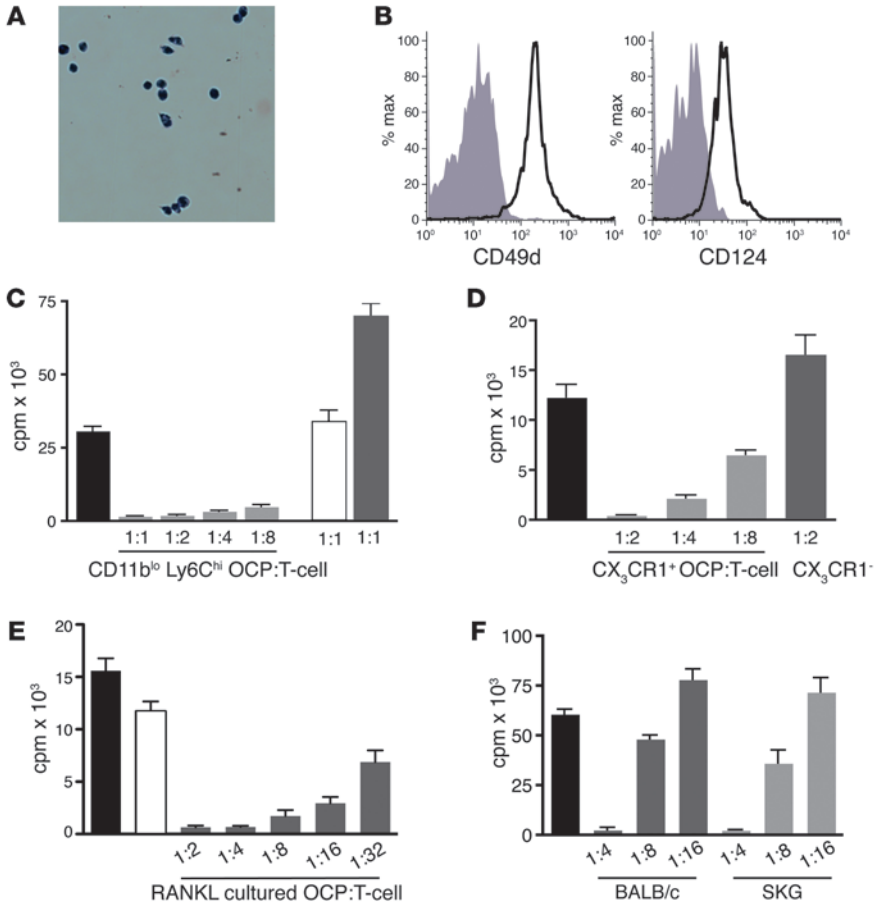

Figure 7
CD11b^{lo}Ly6C^{hi} OCPs have cell-surface markers of MDSCs and suppress in vitro T cell proliferation. (**A**) Wright-Giemsa stain of sorted OCPs cultured for 48 hours in M-CSF demonstrates monocytic nuclear morphology and characteristic gray blue cytoplasm. Original magnification, ×20. (**B**) Similar to MDSCs, BM CD11b^{lo}Ly6C^{hi} OCPs are CD49d and CD124 positive. Antibody-specific staining of cells gated on CD3$^-$B220$^-$Ter119$^-$CD11b$^{-/lo}$Ly6C^{hi} is shown in black line, isotype staining in gray area. (**C**) CD11b$^{-/lo}$Ly6C^{hi} OCPs purified from SKG BM suppress CD4$^+$ T cell proliferation (light gray bars) in contrast with CD11b$^+$Ly6C$^+$ (white bar) or QN (dark gray bar) populations from the same BM. Data are representative of 3 independent experiments. (**D**) CD11b^{lo}Ly6C^{hi} OCPs sorted from C57BL/6 CX$_3$CR1:GFP^{het} BM based on CX$_3$CR1 expression demonstrate that, similar to osteoclast precursor potential, suppressor activity is seen in the CX$_3$CR1$^+$ (light gray bars) but not CX$_3$CR1$^-$ (dark gray bar) population. (**E**) Inhibition of T cell proliferation by freshly isolated OCPs is maintained after differentiation of sorted OCPs in the presence of M-CSF and 100 ng/ml RANKL for 4 days. Addition of RANKL to proliferation medium does not significantly inhibit proliferation (white bar), whereas cultured OCPs retain suppressive activity (gray bars). (**F**) There is no significant difference in suppressor activity between OCPs derived from BALB/c mice (dark gray bars) and those from arthritic SKG mice (light gray bars).

degree than Tregs (Figure 6D). Joint histology showed decreased inflammation in the group receiving OCPs (Figure 6E) compared with CD4$^+$ T cells. Thus, OCPs demonstrate immunomodulatory activity in an in vivo arthritis model.

The OCP group had clinically less severe arthritis and the percentage of IL-17–producing CD4$^+$ T cells isolated from lymph nodes was decreased (Supplemental Figure 6B). However, systemic inflammation remained high, as measured by serum levels of TNF-α, IL-6, and IL-1 (Supplemental Figure 6C). This is possibly explained by observation that OCPs exacerbated the inflammatory skin disease previously reported by others that develops when the CD4$^+$ T cells are adoptively transferred into immunodeficient mice (Supplemental Figure 6, D and E, and refs. 37, 38).

OCPs have characteristics of MDSCs and suppress T cell proliferation in vitro. The unexpected immunomodulatory activity, high Ly6C expression, and mixed M1/M2-like cell-surface phenotype of OCPs was reminiscent of M-MDSCs (39). We thus investigated whether OCPs have other characteristics of monocytic MDSCs. Wright-Giemsa stain of purified OCPs demonstrated that they have monocytic morphology (Figure 7A), similar to Ly6C^{hi} MDSCs. OCPs also expressed CD49d and CD124/IL4Ra, consistent with the described cell-surface phenotype of MDSCs (Figure B and refs. 40, 41).

We next tested whether OCPs have T cell–suppressive activity in vitro. Proliferation of wild-type BALB/c CD4$^+$ T cells stimulated by plate-bound anti-CD3/CD28 antibodies was efficiently suppressed by the addition of purified SKG BM OCPs to the culture (Figure 7C). OCPs were also able to suppress CD8$^+$ T cell proliferation (Supplemental Figure 7). In contrast, CD11b$^+$Ly6C^{int} or QN populations isolated from the same BM lacked suppressive activity (Figure 7C). Although the population falling within the CD11b$^{-/lo}$Ly6C^{hi} gate contained osteoclast progenitors and the capacity to suppress T cell proliferation, it is possible that these disparate functions reside within different subpopulations. To address this possibility, we further divided the CD11b$^{-/lo}$Ly6C^{hi} population based on CX$_3$CR1 expression and found that suppressive activity, such as osteoclast progenitor function, was restricted to the CX$_3$CR1$^+$ population (Figure 7D). Furthermore, after differentiation of purified OCPs in M-CSF and RANKL, the population retained suppressive activity (Figure 7E), arguing for both suppressor and OCP functions residing within the same population.

SKG OCPs are similar to wild-type OCPs in their ability to suppress CD4$^+$ T cells. CD11b$^{-/lo}$Ly6C^{hi} OCPs expand in SKG arthritis and have T cell–suppressive activity in vitro and immunomodulatory activity in vivo, yet are not sufficient to prevent the development of zymosan-induced SKG arthritis. We thus asked whether OCPs derived from arthritic SKG mice differ in their suppressive activity from BALB/c mice. We found that CD11b$^{-/lo}$Ly6C^{hi} OCPs isolated from arthritic SKG mice are equivalent to wild-type BALB/c mice in their in vitro suppressive activity (Figure 7F).

Suppression of T cell proliferation by OCPs is mediated by NO and requires T cell–derived IFN-γ stimulation of OCPs. As CD11b$^{-/lo}$Ly6C^{hi} OCPs appeared to share many of the characteristics of MDSCs, we investigated whether OCPs are similar to MDSCs in mechanisms of T cell suppression. We first examined whether cell-cell contact is required

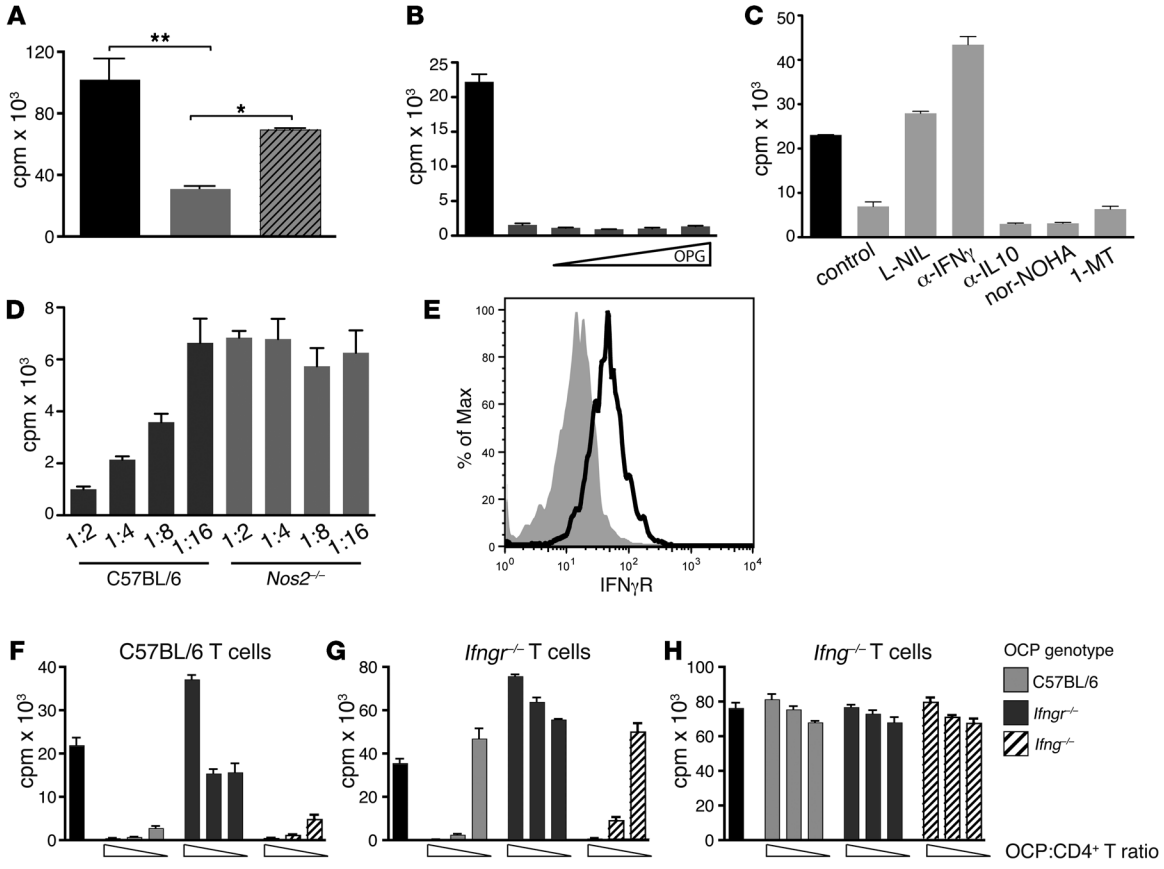

Figure 8

Suppression of CD4+ T cell proliferation by CD11b^{lo}Ly6C^{hi} OCPs requires NOS2, caspase activity, and IFN-γ. (**A**) Full suppression of T cell proliferation requires cell-cell contact. Maximal CD4+ T cell proliferation (black bars) is inhibited by CD11b$^{-/lo}$Ly6C^{hi} OCPs in the lower chamber (gray bars) more efficiently than OCPs in upper chamber (striped) in Transwell assays.**P = 0.02; *P = 0.035. (**B**) Suppression of T cell proliferation by OCP is not relieved by OPG. A ratio of 1:4 OCP/T cell inhibits proliferation (gray bars) compared with T cells alone (black bars). OPG at concentrations from 25–200 ng/ml had no effect. (**C**) CD4+ T cell proliferation (black bars) is suppressed by OCPs at a ratio of 1:4 (gray bars). The addition of the NOS2 inhibitor L-NIL or blocking antibody to IFN-γ relieves suppression compared with isotype/DMSO control. Inhibition of IL-10, arginase, and IDO have no effect. (**D**) OCPs from *Nos2*$^{-/-}$ mice (light gray bars) have decreased T cell–suppressive activity compared with C57BL/6 OCPs (dark gray bars). (**E**) OCPs express the IFN-γ receptor α-chain (black line) compared with isotype control (gray area). (**F**–**H**) T cell–derived IFN-γ and intact IFN-γ signaling in OCPs is required for suppression. (**F**) Proliferation of wild-type CD4+ T cells (black bar) is suppressed by OCP derived from C57BL/6 (light gray bars) or *Ifng*$^{-/-}$ mice (striped bars) over a range of ratios from 1:2 to 1:8. In contrast, OCPs derived from *Ifngr*$^{-/-}$ mice (dark gray bars) do not suppress. (**G**) Proliferation of *Ifngr*$^{-/-}$ CD4+ T cells (black bar) is similarly inhibited by wild-type and *Ifng*$^{-/-}$ OCPs, but not *Ifngr*$^{-/-}$ OCP *Ifng*$^{-/-}$. (**H**) Proliferation of *Ifng*$^{-/-}$ T cells (black bar) is not inhibited by OCPs of any genotype.

for suppressive activity utilizing Transwell chambers. Addition of OCPs to the bottom chamber, in contact with T cells, suppressed T cell proliferation as expected. Suppressive activity was significantly decreased, but not completely abrogated when OCPs were added to the top chamber (Figure 8A). Thus, although full suppressive activity requires cell-cell contact, the suppression mechanism likely also involves diffusible mediators. Th17 cells promote osteoclastogenesis via membrane-bound RANKL (42), and one candidate for a cell contact–dependent mechanism could involve RANKL-RANK signaling. However, addition of recombinant OPG, a decoy receptor for RANKL, to cocultures did not alter suppression (Figure 8B), although it effectively inhibited RANKL-induced osteoclastogenesis (J.F. Charles, unpublished observations).

To further investigate the mechanism of suppression, we tested a panel of inhibitors to interrogate candidate pathways based on previous studies of MDSCs. In the 2 autoimmune models where MDSCs have been identified, suppression depends on IFN-γ and NO (43, 44). Suppression of T cell proliferation by CD11b$^{-/lo}$Ly6C^{hi} OCPs was efficiently inhibited by the inclusion of N6-(1-iminoethyl)-L-lysine (L-NIL), a specific inhibitor of NOS2, in the culture and by blocking antibodies to IFN-γ (Figure 8C). In contrast, antibody blockade of IL-10 or inhibitor nor-NOHA (an ihibitor of arginase) or 1-methyl tryptophan (1-MT, an inhibitor of indoleamine-pyrrole 2,3-dioxygenase [IDO]) had no effect on suppression. Consistent with inhibition of suppression seen with the addition of L-NIL, OCPs from *NOS*$^{-/-}$ mice did not suppress CD4+ T cell proliferation as efficiently as wild-type OCPs (Figure 8D). NO synthase is induced downstream of IFN-γ receptor activation, and OCPs expressed IFN-γR (Figure 8E). IFN-γ signaling in OCPs is required for suppression, as the proliferation of wild-type and *Ifngr*$^{-/-}$ CD4+ T cells could be suppressed by *Ifng*$^{-/-}$ but not *Ifngr*$^{-/-}$ OCPs (Figure 8, F–H). In contrast, suppression of

T cell proliferation by OCPs requires IFN-γ production by T cells. as demonstrated by the finding that *Ifng*$^{-/-}$ CD4$^+$ T cells are not suppressed by OCPs of any genotype (Figure 8, F–H).

Discussion

We have identified a CD11b$^{-/lo}$Ly6C^{hi}CX$_3$CR1$^+$ population in BM with dual OCP and MDSC function. This population is the predominant source of osteoclasts in BM cultures and is distinct from other myeloid precursors based on its cell-surface phenotype. We further show that CD11b$^{-/lo}$Ly6C^{hi} OCPs give rise to bone adherent, cathepsin K, and TRAP-expressing multinucleated osteoclasts in vivo and are thus are a bona fide OCPs.

The OCPs described in this study are phenotypically distinct from previously described MDP, CDP, and monocyte populations, suggesting that OCPs are a unique precursor population analogous to CDPs. It is likely, however, that some plasticity exists between OCPs and other myeloid phenotypes, as suggested by the in vitro findings that immature DCs can give rise to osteoclasts and our findings that OCPs can differentiate into macrophages or DCs in the appropriate cytokine environment. Interestingly, MDSCs are reported to appear transiently in BM cultures for DCs under some conditions. Somewhat similar to OCPs in this study, the MDSCs in DC cultures are Ly-6C$^+$CD11b$^+$CD11c$^-$ (45). It would be of interest to determine whether in DC cultures this cell type gives rise to both MDSCs and osteoclasts.

It has previously been suggested that increased OCP frequency contributes to bone loss and erosions in inflammatory arthritis. Consistent with this, we observe that OCP cells increase in the BM in mouse models of inflammatory erosive arthritis. However, adoptive transfer experiments demonstrated that cotransfer of OCPs with SKG CD4$^+$ T cells to a *Rag2*$^{-/-}$ recipient markedly decreases arthritis severity. These findings suggest that the CD11b$^{-/lo}$Ly6C^{hi} OCP population is also immunomodulatory. Phenotypically CD11b$^{-/lo}$Ly6C^{hi} OCPs share many characteristics of M-MDSCs, including a mixed M1- and M2-like phenotype and the ability to suppress T cells using a NO-dependent mechanism.

The OCP population identified here, however, is not phenotypically uniform, as demonstrated by heterogeneity of expression for CD11b, CD117, and Ki67, and variability in the osteoclastogenic potential of single-cell clones. Thus, we cannot rule out the possibility that while both functions reside within the OCP population, they do not reside in a single cell. Using current cell-surface markers, we have not been able to further subdivide this population into distinct functional subsets, and the maintenance of T cell suppression after differentiation to osteoclasts suggests that one cell type has the capacity to develop multiple functional activities. Consistent with this, a recent study found that mature human osteoclasts can suppress T cell proliferation in vitro (46).

The inflammatory microenvironment affects osteoclast differentiation via the actions of multiple cytokines. TNF-α and IL-6 produced by synovial macrophages and Th17-derived IL-17 all act to increase RANKL on osteoblasts and synovial fibroblasts, and TNF-α, IL-1, and IL-6 can directly affect osteoclast differentiation (22, 47). Several studies suggest that OCPs are also altered by inflammation. Increased circulating OCPs can be detected in psoriatic arthritis and RA patients (20, 48). In the hTNF-α–Tg murine arthritis model, both BM and peripheral blood OCPs were increased in arthritic mice, as we see in the present study. Thus, bone loss and erosions in inflammatory arthritis may result from a synergy between increased precursors and a more prodifferentiation microenvironment. Interestingly, osteoclast differentiation is inhibited by IFN-γ, yet IFN-γ is required for OCPs to suppress T cells. Thus, exposure to IFN-γ may function to skew CD11b$^{-/lo}$Ly6C^{hi} cells toward a primarily MDSC function. In contrast, exposure of the OCP population to M-CSF and RANKL stimulates osteoclastogenesis, but does not eliminate MDSC function.

IFN-γ likely has complex effects on basal bone turnover beyond pure osteoclast inhibition. Although bone mass is decreased in *Ifngr*$^{-/-}$ mice, this appears to be primarily a defect in bone formation, and osteoclast number is not increased (49). Neither IFN-γ nor IFN-γR deficiency substantially affected BM OCP frequency or number (J.F. Charles, unpublished observations). In inflammatory conditions, however, a clear proosteoclast effect of IFN-γR deficiency is seen, with increased osteoclast formation and erosion after LPS injection (50). The effect of IFN-γR deficiency may be most evident after an inflammatory stimulus, where the OCP population is both increased and biased toward an osteoclast fate rather than MSDC function due to the inability to respond to IFN-γ.

Whether the CD11b$^{-/lo}$Ly6C^{hi} myeloid precursor population differentiates toward an MDSC or osteoclast functionality may also be dependent on other innate signals in the environment. Interestingly, deficiency in PIR-B was recently shown to decrease MDSC function in the periphery in a tumor model (39) and has also been shown to increase osteoclast differentiation in vitro (31). Although no effect of PIR-B deficiency on basal bone parameters was seen, it is possible that the role of innate immune receptors such as PIR-B in regulating osteoclast differentiation is context dependent.

Although initially described as a tumor-induced population, an increase in MDSCs was recently found in mouse models of autoimmune disease and in humans with ulcerative colitis (43). Ly6C^{hi}Ly6G$^-$ splenic MDSCs are induced in EAE (44). Similarly, CD11b$^+$Gr1$^+$ MDSCs with both in vitro and in vivo suppressive activity are induced in spleen and intestine in a mouse model of colitis (43). Expansion of MDSC populations in chronic inflammatory conditions may be one of many mechanisms for fine-tuning immune system activation, although the physiologic importance of this mechanism for autoimmune disease is only beginning to be defined. In the SKG autoimmune arthritis model, induction of an OCP population with MDSC activity in arthritic mice was not sufficient for disease control. MDSC function of OCPs may be incompletely effective for a number of reasons, including inadequate number, lack of colocalization with pathogenic T cells, resistance of SKG T cells to suppression, insufficient T cell production of IFN-γ, or some combination of these factors.

MDSCs have been demonstrated to induce expansion of Tregs in a tumor model, a function that is diminished if MDSCs are skewed toward an M1 phenotype by loss of PIR-B (39). It is possible that high levels of TNF-α, IL-1, and IL-6 produced by synovial fibroblasts bias the CD11b$^{-/lo}$Ly6C^{hi}CX$_3$CR1$^+$ OCP population toward a more M1 phenotype in the periphery, altering their peripheral MDSC functionality without changing the suppressive properties of BM OCPs. The cytokine environment could also bias OCPs toward osteoclast differentiation such that systemic bone loss and erosive disease is a by-product of the immune system's failed attempt at homeostasis.

Artificially increasing CD11b$^{-/lo}$Ly6C^{hi} OCPs to approximately 5-fold their normal number decreased joint inflammation in the SKG adoptive transfer model. Skin inflammation was not ameliorated, however, and was even exacerbated. Skin inflammation after adoptive transfer of naive T cells into *scid/scid* mice has been

previously described (37, 38). As cell-cell contact is required for full T cell suppression by OCPs, the differential effect on inflammation at distinct sites may relate to localization of adoptively transferred OCPs and/or the local cytokine environment that may influence the suppressive capacity of OCPs.

In contrast with the adoptive transfer model, the increase in $CD11b^{-/lo}Ly6C^{hi}$ OCPs after zymosan injection does not suppress the development of SKG inflammatory arthritis in response to zymosan. It may be that the OCP number is inadequate in the physiologic setting or that they do not localize in adequate proximity to T cells to substantially alter disease activity. In the adoptive transfer model of inflammatory arthritis using SKG T cells, OCPs and T cells were transferred to the RAG2-deficient recipient together, ensuring colocalization that may have been critical for the observed immunomodulatory effect. Although SKG OCPs are equivalent to BALB/c OCPs in T cell–suppressive activity in vitro, we cannot rule out the possibility that, particularly in vivo, SKG T cells may be less susceptible to suppression, may not consistently produce the IFN-γ required for MDSC activity, or that additional cell types prevent OCPs from suppressing the development of inflammatory arthritis.

The MDSC function of the OCP population is similar to monocytic MDSCs described in other autoimmune models. However, OCPs likely represent only a subset of MDSCs. In the OCP population, suppression of T cell proliferation is dependent on IFN-γ and NO. MDSCs are a heterogeneous population, and other MDSCs suppress T cells via arginase-dependent pathways or inhibitory cytokine secretion. In addition, the OCP population was not the only suppressive myeloid population seen in the BM of mice with inflammatory arthritis. We also observed that a $CD11b^{+}Ly6C^{hi}$ population could suppress T cell proliferation in vitro, though these cells did not show osteoclastogenic potential (J.F. Charles, unpublished observations). Thus while the $CD11b^{-/lo}Ly6C^{+}$ OCP population has MDSC function, not all MDSCs are OCPs.

The outcome of the interaction between OCPs and T cells will also differ depending on the subset of T cells and the environment in which they are interrogated. Th17 cells promote osteoclast differentiation via induction of RANKL on stromal cells, as well as surface RANKL on Th17 cells themselves, whereas Th1 cell production of IFN-γ results in inhibited osteoclast differentiation, although they also express RANKL (42, 50). Our results suggest that Th1 cells producing IFN-γ would activate T cell–suppressive activity by OCP cells. The effect of Th17 cells and IL-17 on MDSC function is not yet known, but may be an additional factor influencing the fate of the OCP population.

Our results demonstrate a dual OCP and MDSC function for the BM $CD11b^{-/lo}Ly6C^{hi}$ population in vitro and in vivo. It is possible that induction of $CD11b^{-/lo}Ly6C^{hi}$ OCPs under inflammatory conditions represents a homeostatic mechanism aimed at dampening T cell activation, which is ineffective in the inflammatory microenvironment, but successfully increases a pool of precursors that can be shunted toward osteoclast differentiation and the formation of erosions. Thus,a more complete understanding of the regulation of the OCP population likely has significance for the regulation of bone loss and autoimmunity.

Methods

Mice. BALB/c SKG mice, a gift of Shimon Sakaguchi (Kyoto University, Kyoto, Japan) were housed in specific pathogen–free conditions at the San Francisco VA Medical Center. Arthritis was induced in 8-week-old female SKG mice by i.p. injection of 2 mg zymosan, and BM OCPs were assessed or isolated at 1 week or 8 weeks after zymosan injection and compared with littermate sex-matched controls injected with PBS (referred to in the text as healthy SKG controls). Female human *TNFA*–Tg heterozygous mice and age- and sex-matched C57BL/6 controls were purchased from Taconic and analyzed at 20 weeks of age. BM of all other genotypes was analyzed at 6–9 weeks of age. C57BL/6 *CX_3CR1-GFP^{het}* mice were bred at the VA from *CX_3CR1*-GFP mice obtained from Jackson. Cathepsin K Cre mice were a gift of Shigeaki Kato (University of Tokyo, Tokyo, Japan). The Cre reporter strain *mT/mG*, *Ccr2*$^{-/-}$, *Ifng*$^{-/-}$, and *Ifngr*$^{-/-}$ mice were purchased from Jackson. Eight-week-old *Nfatc1*$^{fl/fl}$ *Mx1-Cre* mice were treated with 250 μg of poly(I:C) given by i.p. injection on days 1, 3, and 5 and the resultant osteoclast-deficient *Nfatc1*$^{Δ/Δ}$ hosts used for OCP transfer 4 weeks after poly(I:C) treatment. The osteoclast-deficient phenotype of these mice has previously been described (35). BALB/c mice were purchased from Simonsen, and C57BL/6 mice were bred at the VAMC. *Rag2*$^{-/-}$ and *Nos2*$^{-/-}$ mice were purchased from Taconic.

Reagents. Recombinant murine M-CSF and RANKL were from PeproTech. GM-CSF was purchased from R&D Systems. Supernatant from CMG 14-22 cells at 5% v/v was used as an alternate source of M-CSF where noted. Wright-Giemsa stain (Sigma-Aldrich) was used according to the manufacturer's instructions. OPG was purchased from R&D. IL-10 (JES 52A5) and IFN-γ (XMG1.2) neutralizing antibodies were obtained from the University of California Hybridoma Core. NOS2 inhibitor L-NIL, caspase inhibitor zVAD-fmk, and arginase 1 inhibitor N^{w}-hydroxyl-nor-L-arginine (nor-NOHA) were purchased from Calbiochem. IDO inhibitor 1-MT, hydroxyurea, *E. coli* LPS, and cytochalasin D were purchased from Sigma-Aldrich. Poly(I:C) was from Amersham. Alex Fluor 488–conjugated zymosan A particles and rhodamine phalloidin were from Invitrogen. All reagents were prepared according to the manufacturers' recommendations.

μCT tomography. After serial fixation in 4% phosphate buffered formaldehyde and 70% ethanol, the proxima tibia and femur were scanned using a vivaCT 40 (Scanco Medical) with a voxel size of 10.5 mm and x-ray energy of 55 kV. A 1.2-mm region of interest was analyzed with segmentation values set at 0.8/1/250, and structural and 3D parameters were calculated using Scanco Medical software. Images of SKG arthritis paws were reconstructed from scans performed with a voxel size of 15 mm and segmentation values of 0.7/1/300. Adoptive transfer experiment paws were scanned using a μCT 35 (Scanco Medical) with a voxel size of 12 mm and segmentation values of 0.8/1/210.

Flow cytometry. BM was flushed with PBS. After hypotonic red cell lysis, cells were blocked with 2.4 G2 antibody followed by incubation with a mix of CD3e, CD45R/B220, and Ter119, all conjugated to FITC or PE (all from eBioscience), Ly6C-PE-Cy7 (clone AL-21; BD Biosciences — Pharmingen), and CD11b-APC (eBioscience). Flow cytometry was performed on a FACSCalibur (BD Biosciences) and analyzed with FlowJo software (Tree Star Inc.). After exclusion of $CD3/B220/Ter119^{+}$ cells, cells were gated based on CD11b and Ly6C staining intensity. Expression of cell-surface markers of monocyte differentiation on $CD11b^{lo}Ly6C^{hi}$ cells was identified using a-CCR2 (MC-21; gift of Mattias Mack), biotin-conjugated CD115, CD117, and CD135 (AFS98, 2B8, A2F10; eBioscience), and Ly6G-PE or –FITC and Gr1-PE (1A8, RB6-8C5; BD Biosciences — Pharmingen). Additional cell-surface markers were examined using CD11c-PE or bio (N418, eBioscience), IFN-γR–bio (GR20; BD Biosciences), Dectin1-PE (2A11; AbD Serotech), CD36-PE (72-1; eBioscience), CD206-PE (MR5D3; AbD Serotech), CD124 (mIL4R-M1; BD Biosciences — Pharmingen), CD49d (R1-2; eBioscience), MDL-1/CLEC5A (226402; R&D Systems), PIRA/B-PE (6C1; BD Biosciences — Pharmingen), and biotinylated TREM2 clone 67.8 prepared as previously described (51). MHCII I-A/I-E-PE (M5/114.15.2) and

F4/80-APC (BM8) were from BioLegend. Ki-67 expression was detected using anti–Ki-67–PE (B56; BD Biosciences — Pharmingen) according to the manufacturer's instructions. RANK expression on OCPs and BM cells cultured in the presence of RANKL and M-CSF for 2 days (D2 OCP) was examined using GST-RANKL-biotin compared with GST-biotin control protein (gift of Hisataka Yasuda, Oriental Yeast Company, Tokyo, Japan) at a concentration of 1 μg/10^6 cells, followed by detection with streptavidin-APC (BioLegend). Specificity of binding was tested by preincubation of cells in the presence of 200 ng/ml RANKL (R&D Systems) for 15 minutes at room temperature prior to staining.

Isolation of OCPs and other BM populations. BM cells prepared as above were incubated with CD45R, B220, and Ter119 MicroBeads (Miltenyi) and run over an AutoMACs column in deplete mode; the negatively selected fraction was subsequently stained for CD11b, Ly6C expression, and in addition, CD3, B220, and Ter119 expression and Sytox Blue (Invitrogen) uptake. Individual cell populations were sorted based on CD11b and Ly6C expression within the B220/CD3/$Ter119^-$ gate utilizing the FACSAria (BD Biosciences) in the Cell Sorting Core at the San Francisco VA Medical Center. In subsequent assessment, the purity of sorted populations ranged from 92% to 99%.

Osteoclast culture and resorption assay. FACS-sorted populations were plated in triplicate at a density between 1 and 25 × 10^3/well on 96-well plates and differentiated in α-MEM containing 10% FBS, 40 ng/ml M-CSF, and 25 ng/ml RANKL for 3 days. Osteoclasts were differentiated from total BM by replating nonadherent BMMs after 24 hours of culture in α-MEM supplemented with 5% v/v CMG at a density of 0.25 × 10^5/well and cultured in 40 ng/ml M-CSF and 25 ng/ml RANKL for 5–6 days. Cells were fixed and stained for TRAPc using the Acid Phosphatase Kit (Sigma-Aldrich) according to the manufacturer's instructions. Digital images acquired at ×10–×16 as noted were cropped and adjusted for brightness, contrast, and color balance using Photoshop CS3. For resorption assays, cells were plated on BioCoat Osteologic slides (BD Biosciences) and maintained in 40 ng/ml M-CSF and 25 ng/ml RANKL for 14 days. Resorption pits were analyzed using Osteologic II software (BioQuant).

OCP transfer and in vivo differentiation. $CD11b^{-/lo}Ly6C^{hi}CD117^+$ OCPs were purified from *mT/mG*^{OC} or C57BL/6 BM by flow cytometry (94%–98% pure) as described above, but omitting the initial depletion step, and resuspended in α-MEM 20% FCS at a concentration of 4 × 10^6/ml. Osteoclast-deficient *nfatc1*$^{\Delta\Delta}$ mice as described above were anesthetized, the distal femur was surgically exposed by medial displacement of the patella, and a 25-gauge needle used to bore a track into the BM cavity. Purified *mTmG*^{OC}, unlabeled C57BL/6 OCP (1 × 10^4) cells, or PBS were injected through a spinal needle inserted into the BM cavity. Injected femurs were harvested 7 days after cell transfer. Alternatively, 8-week-old C57BL/6 mice were injected with LPS, 25 mg/kg body weight, into their cranial suture. 24 hours after LPS calvarial injection, 5 × 10^4 purified *mT/mG*^{OC} OCP or PBS were administered intravenously. Calvaria were harvested 5 days after cell transfer.

Histology. Long bones and calvaria were decalcified in 0.5 M EDTA/citric acid solution. GFP was detected by immunohistochemistry with rabbit anti-GFP antibody (Abcam) on trypsin-digested, paraffin-embedded sections, followed by biotinylated goat anti-rabbit and streptavidin-HRP (both from Vector labs) and developed with DAB (Sigma-Aldrich). TRAP staining was performed as previously described (52). Sections were counterstained with hematoxylin Gil-3 (Sigma-Aldrich).

Adoptive transfer into Rag2$^{-/-}$ *mice*. Conventional $CD4^+$ T cells ($CD4^+CD25^-$) from SKG mice and Tregs ($CD4^+CD25^-$) from wild-type mice were purified by MACS columns according to the manufacturer's instructions (Miltenyi Biotec). 4 × 10^5 conventional SKG $CD4^+$ T cells were either transferred alone or cotransferred in 1:1 ratio with either wild-type Tregs or $CD11b^{-/lo}Ly6C^{hi}$ OCPs purified as above (94% pure) into *Rag2*$^{-/-}$ mice. Mice were assessed for clinical signs of arthritis weekly, and at 4 weeks, arthritis was scored by a blinded assessor and mice were euthanized. Arthritis scoring was modified from the published scoring system for SKG mice by the addition of 0.1 point for mild large joint inflammation (14). Scoring of erosions on a scale of 0–4 was performed by a blinded observer provided with cross-sectional μCT images taken every 0.12 mm from the end of the tibia to the metatarsal joints and presented in scrambled order. Total erosion score was averaged over the number of images scored for each mouse to correct for variability in the number of images covering the anatomical distance (30–34 slices, 3.6–4 mm). Skin was similarly scored by a blinded assessor on a scale of 0–4 each for severity of facial, extremity, and ear inflammation for a summary score of 0–12.

Cytokine and CTX assays. Serum cytokines were assayed using BioPlex mouse cytokine assays (Bio-Rad). Serum C-terminal fragments of CTX were quantified using the RatLaps EIA assay (Immunodiagnostics Systems).

Suppression assays. Splenic $CD4^+$ T cells were purified using the $CD4^+$ T cell Isolation Kit (Miltenyi) run over an AutoMACs column in deplete-s mode, and purity was confirmed to be greater than 90% by flow cytometric analysis. Splenic $CD8^+$ T cells were isolated by sorting for $CD3^+CD8^+$ cells on the FACSAria. T cells were plated in wells coated with antibodies to CD3 and CD28 (2C11, 37.51; BD Pharmingen) at a density of 25 × 10^3/well in proliferation medium (RPMI supplemented with 10% FBS, 5 × 10^{-5}M β-mercaptoethanol, sodium pyruvate, and nonessential amino acids). After 24 hours, purified OCPs (or other populations) prepared as described above, were resuspended in proliferation medium and added to T cell cultures at the ratio of OCP to T cells ranging from 1:2 to 1:16. After 48 hours, cells were pulsed with 1 mCi of ^{3}H-thymidine (Amersham) diluted in proliferation medium, and assays were harvested at 12–16 hours. Mechanism of suppression was examined using a panel of specific inhibitors. In these assays, inhibitors were added to the assays at the time of OCP addition. OPG was added over a concentration range of 25–200 ng/ml. Other inhibitors were added to a final concentration of 100 mM zVAD-fmk, 1 mM 1-MT, 0.5 mM nor-NOHA, 0.5 mM L-NIL, or 20 mg/ml neutralizing antibody to IFN-γ or IL-10. Control assay contained DMSO plus 20 mg/ml rat IgG.

Statistics. Data represent mean ± SEM. Analysis was performed using GraphPad Prism, version 5. Statistical significance was assessed using a 2-tailed Student's *t* test, Mann-Whitney test, or 1-way ANOVA, as indicated in the figure legends, considering a P value ≤ 0.05 as significant.

Study approval. All animal experiments were conducted in accordance with the Association for Assessment and Accreditation of Laboratory Animal Care. Protocols were approved by the IACUC at the VAMC, IACUC at the University of California, San Francisco, California, USA, or the Standing Committee on Animals at Harvard, as appropriate.

Acknowledgments

We are grateful to S. Sakaguchi and S. Kato for providing the SKG and cathepsin K Cre mice, respectively. Rubi Gribi, Debra A. Cheng, and Dorothy Hu provided invaluable technical assistance. We thank Mehrdad Matloubian for helpful discussions and comments on the manuscript, and the SFVA Flow Cytometry Core, the μCT core facilities at the San Francisco VA Medical Center and Harvard School of Public Health, and the Rodent Histology Core at Harvard Medical School for technical assistance. This work was supported by an American College of Rheumatology Research and Education Foundation Rheumatology Investigator Award (to J.F. Charles); NIH training grant F32 AR056174-03 (to L-.Y. Hsu); NIH grants K08AR054859 and R01AR060363 and a Career Award for Medical Scientists from the Burroughs Wellcome Fund (to A.O. Aliprantis): and a VA Merit Review award and NIH

grant AR050038 administered by the Northern California Institute for Research and Education (to M.C. Nakamura). The VAMC, San Francisco, California, USA, and the Rosalind Russell Medical Research Center for Arthritis provided additional support.

Address correspondence to: Julia F. Charles, 75 Francis Street, Smith Building 614, Boston, Massachusetts 02115, USA. Phone: 415.690.6047; Fax: 617.432.6452; E-mail: jfcharles@partners.org.

Received for publication September 8, 2011, and accepted in revised form September 6, 2012.

Julia F. Charles's present address is: Department of Medicine, Harvard Medical School, Boston, Massachusetts, USA.

1. Kong YY, et al. OPGL is a key regulator of osteoclastogenesis, lymphocyte development and lymph-node organogenesis. *Nature*. 1999;397(6717):315–323.
2. Dougall WC, et al. RANK is essential for osteoclast and lymph node development. *Genes Dev*. 1999;13(18):2412–2424.
3. Li J, et al. RANK is the intrinsic hematopoietic cell surface receptor that controls osteoclastogenesis and regulation of bone mass and calcium metabolism. *Proc Natl Acad Sci U S A*. 2000;97(4):1566–1571.
4. Kodama H, et al. Congenital osteoclast deficiency in osteopetrotic (op/op) mice is cured by injections of macrophage colony-stimulating factor. *J Exp Med*. 1991;173(1):269–272.
5. Felix R, Cecchini MG, Fleisch H. Macrophage colony stimulating factor restores in vivo bone resorption in the op/op osteopetrotic mouse. *Endocrinology*. 1990;127(5):2592–2594.
6. Arai F, et al. Commitment and differentiation of osteoclast precursor cells by the sequential expression of c-Fms and receptor activator of nuclear factor kappaB (RANK) receptors. *J Exp Med*. 1999;190(12):1741–1754.
7. Jacquin C, Gran DE, Lee SK, Lorenzo JA, Aguila HL. Identification of multiple osteoclast precursor populations in murine bone marrow. *J Bone Miner Res*. 2006;21(1):67–77.
8. Fogg DK, et al. A clonogenic bone marrow progenitor specific for macrophages and dendritic cells. *Science*. 2006;311(5757):83–87.
9. Geissmann F, Manz MG, Jung S, Sieweke MH, Merad M, Ley K. Development of monocytes, macrophages, and dendritic cells. *Science*. 2010; 327(5966):656–661.
10. Miyamoto T, et al. Bifurcation of osteoclasts and dendritic cells from common progenitors. *Blood*. 2001;98(8):2544–2554.
11. Yao Z, et al. Tumor necrosis factor-alpha increases circulating osteoclast precursor numbers by promoting their proliferation and differentiation in the bone marrow through up-regulation of c-Fms expression. *J Biol Chem*. 2006;281(17):11846–11855.
12. Muto A, et al. Lineage-committed osteoclast precursors circulate in blood and settle down into bone. *J Bone Miner Res*. 2011;26(12):2978–2990.
13. Speziani C, et al. Murine dendritic cell transdifferentiation into osteoclasts is differentially regulated by innate and adaptive cytokines. *Eur J Immunol*. 2007;37(3):747–757.
14. Sakaguchi N, et al. Altered thymic T-cell selection due to a mutation of the ZAP-70 gene causes autoimmune arthritis in mice. *Nature*. 2003; 426(6965):454–460.
15. Yoshitomi H, et al. A role for fungal {beta}-glucans and their receptor Dectin-1 in the induction of autoimmune arthritis in genetically susceptible mice. *J Exp Med*. 2005;201(6):949–960.
16. Hata H, et al. Distinct contribution of IL-6, TNF-alpha, IL-1, and IL-10 to T cell-mediated spontaneous autoimmune arthritis in mice. *J Clin Invest*. 2004;114(4):582–588.
17. Caetano-Lopes J, et al. Chronic arthritis leads to disturbances in the bone collagen network. *Arthritis Res Ther*. 2010;12(1):R9.
18. Keller KK, Stengaard-Pedersen K, Dagnaes-Hansen F, Nyengaard JR, Sakaguchi S, Hauge EM. Histological changes in chronic autoimmune SKG-arthritis evaluated by quantitative three-dimensional stereological estimators. *Clin Exp Rheumatol*. 2011;29(3):536–543.
19. Walsh NC, et al. Osteoblast function is compromised at sites of focal bone erosion in inflammatory arthritis. *J Bone Miner Res*. 2009;24(9):1572–1585.
20. Ritchlin CT, Haas-Smith SA, Li P, Hicks DG, Schwarz EM. Mechanisms of TNF-alpha- and RANKL-mediated osteoclastogenesis and bone resorption in psoriatic arthritis. *J Clin Invest*. 2003;111(6):821–831.
21. Park-Min KH, et al. Negative regulation of osteoclast precursor differentiation by CD11b and beta2 integrin-BCL6 signaling [published online ahead of print August 14, 2012]. *J Bone Miner Res*. doi:10.1002/jbmr.1739.
22. Takayanagi H. New immune connections in osteoclast formation. *Ann N Y Acad Sci*. 2010;1192:117–123.
23. Ishii M, et al. Sphingosine-1-phosphate mobilizes osteoclast precursors and regulates bone homeostasis. *Nature*. 2009;458(7237):524–528.
24. Maitra R, et al. Dendritic cell-mediated in vivo bone resorption. *J Immunol*. 2010;185(3):1485–1491.
25. Gordon S, Taylor PR. Monocyte and macrophage heterogeneity. *Nat Rev Immunol*. 2005;5(12):953–964.
26. Mosser DM, Edwards JP. Exploring the full spectrum of macrophage activation. *Nat Rev Immunol*. 2008;8(12):958–969.
27. Humphrey MB, et al. TREM2, a DAP12-associated receptor, regulates osteoclast differentiation and function. *J Bone Miner Res*. 2006;21(2):237–245.
28. Paloneva J, et al. DAP12/TREM2 deficiency results in impaired osteoclast differentiation and osteoporotic features. *J Exp Med*. 2003;198(4):669–675.
29. Peng Q, Malhotra S, Torchia JA, Kerr WG, Coggeshall KM, Humphrey MB. TREM2- and DAP12-dependent activation of PI3K requires DAP10 and is inhibited by SHIP1. *Sci Signal*. 2010; 3(122):ra38.
30. Joyce-Shaikh B, et al. Myeloid DAP12-associating lectin (MDL)-1 regulates synovial inflammation and bone erosion associated with autoimmune arthritis. *J Exp Med*. 2010;207(3):579–589.
31. Mori Y, et al. Inhibitory immunoglobulin-like receptors LILRB and PIR-B negatively regulate osteoclast development. *J Immunol*. 2008;181(7):4742–4751.
32. Ochi S, et al. Pathological role of osteoclast costimulation in arthritis-induced bone loss. *Proc Natl Acad Sci U S A*. 2007;104(27):11394–11399.
33. Richie Ehrlich LI, Serwold T, Weissman IL. In vitro assays misrepresent in vivo lineage potentials of murine lymphoid progenitors. *Blood*. 2011;117(9):2618–2624.
34. Muzumdar MD, Tasic B, Miyamichi K, Li L, Luo L. A global double-fluorescent Cre reporter mouse. *Genesis*. 2007;45(9):593–605.
35. Aliprantis AO, et al. NFATc1 in mice represses osteoprotegerin during osteoclastogenesis and dissociates systemic osteopenia from inflammation in cherubism. *J Clin Invest*. 2008;118(11):3775–3789.
36. Sakaguchi S, Sakaguchi N, Yoshitomi H, Hata H, Takahashi T, Nomura T. Spontaneous development of autoimmune arthritis due to genetic anomaly of T cell signal transduction: Part 1. *Semin Immunol*. 2006;18(4):199–206.
37. Ma HL, et al. IL-22 is required for Th17 cell-mediated pathology in a mouse model of psoriasis-like skin inflammation. *J Clin Invest*. 2008;118(2):597–607.
38. Schon MP, Detmar M, Parker CM. Murine psoriasis-like disorder induced by naive CD4+ T cells. *Nat Med*. 1997;3(2):183–188.
39. Ma G, et al. Paired Immunoglobin-like receptor-B regulates the suppressive function and fate of myeloid-derived suppressor cells. *Immunity*. 2011;34(3):385–395.
40. Youn JI, Nagaraj S, Collazo M, Gabrilovich DI. Subsets of myeloid-derived suppressor cells in tumor-bearing mice. *J Immunol*. 2008;181(8):5791–5802.
41. Haile LA, Gamrekelashvili J, Manns MP, Korangy F, Greten TF. CD49d is a new marker for distinct myeloid-derived suppressor cell subpopulations in mice. *J Immunol*. 2010;185(1):203–210.
42. Sato K, et al. Th17 functions as an osteoclastogenic helper T cell subset that links T cell activation and bone destruction. *J Exp Med*. 2006; 203(12):2673–2682.
43. Haile LA, et al. Myeloid-derived suppressor cells in inflammatory bowel disease: a new immunoregulatory pathway. *Gastroenterology*. 2008;135(3):871–881.
44. Zhu B, et al. CD11b+Ly-6C(hi) suppressive monocytes in experimental autoimmune encephalomyelitis. *J Immunol*. 2007;179(8):5228–5237.
45. Rossner S, Voigtlander C, Wiethe C, Hanig J, Seifarth C, Lutz MB. Myeloid dendritic cell precursors generated from bone marrow suppress T cell responses via cell contact and nitric oxide production in vitro. *Eur J Immunol*. 2005;35(12):3533–3544.
46. Grassi F, et al. T cell suppression by osteoclasts in vitro. *J Cell Physiol*. 2011;226(4):982–990.
47. Karmakar S, Kay J, Gravallese EM. Bone damage in rheumatoid arthritis: mechanistic insights and approaches to prevention. *Rheum Dis Clin North Am*. 2010;36(2):385–404.
48. Gengenbacher M, Sebald HJ, Villiger PM, Hofstetter W, Seitz M. Infliximab inhibits bone resorption by circulating osteoclast precursor cells in patients with rheumatoid arthritis and ankylosing spondylitis. *Ann Rheum Dis*. 2008;67(5):620–624.
49. Duque G, et al. Interferon gamma plays a role in bone formation in vivo and rescues osteoporosis in ovariectomized mice. *J Bone Miner Res*. 2011;26(7):1472–1483.
50. Takayanagi H, et al. T-cell-mediated regulation of osteoclastogenesis by signalling cross-talk between RANKL and IFN-gamma. *Nature*. 2000;408(6812):600–605.
51. Hsieh CL, et al. A role for TREM2 ligands in the phagocytosis of apoptotic neuronal cells by microglia. *J Neurochem*. 2009;109(4):1144–1156.
52. Erlebacher A, Derynck R. Increased expression of TGF-beta 2 in osteoblasts results in an osteoporosis-like phenotype. *J Cell Biol*. 1996;132(1–2):195–210.